OUKA
The University of Osaka
Institutional Knowledge Archive

Title	Neural mechanism of experience-dependent sensory gain control in C. elegans
Author(s)	池尻, 洋輔
Citation	大阪大学, 2023, 博士論文
Version Type	VoR
URL	https://doi.org/10.18910/92178
rights	
Note	

The University of Osaka Institutional Knowledge Archive : OUKA

https://ir.library.osaka-u.ac.jp/

The University of Osaka

Doctoral Thesis

Neural mechanism of experience-dependent sensory gain control in *C. elegans*

Yosuke Ikejiri

Department of Biological Sciences

Graduate School of Science

Osaka University

March 2022

Contents

SUMMARY..... -1-

INTRODUCTION..... -2-

MATERIALS AND METHODS..... - 8-

RESULTS..... -16-

DISCUSSION..... -24-

REFERENCES..... -31-

FIGURES AND TABLES..... -41-

ACKNOWLEGDEMENT..... -63-

PUBLICATIONS AND PRESENTATIONS..... -64-

SUMMARY

Animals' sensory systems adjust their responsiveness to environmental stimuli that vary greatly in their intensity. Here I report the neural mechanism of experience-dependent sensory adjustment, especially gain control, in the ASH nociceptive neurons in *Caenorhabditis elegans*. Using calcium imaging under gradual changes in stimulus intensity, I found that the ASH neurons of naive animals responded to concentration increases in a repulsive odor 2-nonanone regardless of the magnitude of the concentration increase. However, after preexposure to the odor, the ASH neurons exhibited significantly weak responses to a small gradual increase in odor concentration while their responses to a large gradual increase remained strong. Thus, preexposure changed the slope of stimulus–response relationships (*i.e.*, gain control). Behavioral analysis suggested that this gain control contributes to the preexposure-dependent enhancement of odor avoidance behavior. Mathematical analysis revealed that the ASH response consisted of fast and slow components, and that the fast component was specifically suppressed by preexposure. In addition, genetic analysis suggested that G protein signaling is required for the fast component. Thus, my integrative study demonstrated how prior experience dynamically modulates stimulus–response relationships in sensory neurons, eventually leading to adaptive modulation of behavior.

INTRODUCTION

The mechanism of sensory modulation

To survive and reproduce, animals possess the ability of detecting environmental information such as foods, mating partners, and enemies. This ability is strongly dependent on their sensory organs. The intensity of those environmental stimuli can vary by a factor of 10^{10}, although the range of neuronal activity is generally limited to a factor of 10^2 (Shapley and Enroth-Cugell, 1984). Thus, animals need to adjust their range of neuronal activity in peripheral and central sensory systems according to stimulus intensity. Such regulation of neuronal responsiveness has been reported in visual, auditory, olfactory, mechanical, and nociceptive systems, in a variety of animal species ranging from invertebrates to vertebrates (Carew et al., 1971; Dragoi et al., 2000; Priebe and Ferster, 2002; Root et al., 2008; Ulanovsky et al., 2003; Woolf and Ma, 2007).

A famous example for sensory modulations is gill-withdrawal reflex in *Aplysia* (Castellucci et al., 1970; Kupfermann et al., 1970; Pinsker et al., 1970). When a mechanical stimulus is applied to siphon in *Aplysia*, the *Aplysia* withdraw its gill and this gill-withdrawal response is decreased by repeated stimulation to siphon. The neural mechanism of this reduced responsiveness is a decrease in excitatory synaptic releases from sensory neurons (Castellucci et al., 1970). In addition, this gill-withdrawal response becomes larger by applying electrical shock to tail at the same timing with mechanical stimulation. This is caused by an increase in synaptic releases from sensory neurons (Kandel, 2001).

Other famous examples are light adaptation and dark adaptation in visual system (Ebrey and Koutalos, 2001; Lamb and Pugh, 2004). Light adaptation is the modulation by which photoreceptors adjust their responsiveness when moving from an environment with low light intensity to an environment with high light intensity. It is caused by a decrease in the amount of rhodopsin which is required for photoreception. On the other hand, dark adaptation is the modulation to adjust their responsiveness when moving from environment with high light intensity to low light intensity, and it is caused by increase in the amount of rhodopsin. These examples show that the sensory modulation includes “adaptation”, which decreases the neuronal responsiveness and “sensitization”, which increases the responsiveness.

A different type of neuronal response modulation from these is sensory gain control. Gain control refers to a modulation that changes the slope of stimulus–response relationships and is different from adaptation or sensitization, which decreases or increases the overall responsiveness (Figure 1). Gain control has been reported to occur in the visual, auditory and somatosensory cortices of mammals and the olfactory circuit of *Drosophila*, and it is likely conserved across taxa (Andersen et al., 1985; Anderson et al., 2017; Azimi et al., 2020; Chance et al., 2002; Ohzawa et al., 1982; Olsen and Wilson, 2008). However, neuronal and/or molecular mechanisms underlying gain control, as well as the effect of gain control on sensory behavior, have not been sufficiently elucidated.

Analysis of the mechanism of sensory modulation using the nematode, *C.elegans*

The nematode *Caenohabditis elegans* (*C. elegans*) is very suitable for elucidating the mechanism of sensory response. Even though *C. elegans* has only 302 neurons (White et al., 1986), the animals show basic neural function such as sensory response, memory, and learning. In addition, genetic analysis can be easily performed, making it easy to measure neuronal response by calcium imaging and to identify genes involved in the modulation of sensory responses. These advantages make it possible to analyze neural activity at neural circuit, cellular, and genetic levels.

The animals respond to various sensory stimuli and these responses are modulated by experience as learning, and the neurons and genes involved in these responses have also been identified (Bargmann, 2006; De Bono and Maricq, 2005; Ferkey et al., 2021; Sasakura and Mori, 2013). For example, it is shown that ASH polymodal neurons respond to one of the aversive stimuli, cupper ion and that this response is decreased by repeated stimulation (Hilliard et al., 2005). In another example, AWA sensory neuron respond to the attractive odorant diacetyl and ODR-10 is the receptor for this odor (Larsch et al., 2013; Sengupta et al., 1996). However most of the previous sensory experiments for physiological analyses of wild-type animals employed step-wise stimuli that were not controlled gradually in a physiologically meaningful manner. In terms of sensory gain control, while some mutant strains are shown to exhibit different sensory gains (Kuhara et al., 2002; Saro et al., 2020), it

has not been clear whether and how sensory gain control contributes to the wild-type animals' sensory behavior, such as navigation under a chemical gradient.

Repulsive odor learning in *C. elegans*

C. elegans avoidance behavior to the odorant 2-nonanone is an ideal experimental paradigm to study the animals' sensory response and experience-dependent modulation. The animals avoid the odor, and this odor avoidance behavior is enhanced by preexposure to the odor for 1 hour as a type of non-associative learning (Figure 2) (Bargmann et al., 1993; Kimura et al., 2010). In previous studies, it was found that the odor avoidance behavior consists of two behavioral states: (1) run, a long period of straight movement, and (2) pirouette, a period of repeated short movements with frequent directional changes (Kimura et al., 2010; Pierce-Shimomura et al., 1999). It was also found that when the animals sense increases or decreases in odor concentration, it promotes pirouettes or runs, respectively (Figure 3A) (Tanimoto et al., 2017).

Calcium imaging of their neuronal activities with gradual changes in the odor concentration by using original microscope system, OSB2 (Figure 3B) revealed that a pair of ASH nociceptive neurons and a pair of AWB olfactory neurons respond to the odor increase and decrease, respectively (Tanimoto et al., 2017). Furthermore, pharmacological, genetic and mathematical analyses of neuronal activities in the Kimura laboratory have demonstrated that slowly increasing intracellular calcium response to a simple gradual odor decrease in AWB

neurons is modeled by the leaky integration of time-differential of odor concentration (see Figure 3C; for leaky integration equation, please see Materials and Methods), which is mainly mediated by continuous influx of calcium ions through the L-type voltage-gated calcium channel (VGCC) EGL-19 (Tanimoto et al., 2017). Pharmacological analysis also suggested that the ASH response to a simple gradual odor increase (odor gradient #1) consists of an AWB-like slow component plus a fast and transient component, which has not been modeled yet (Figure 3D) (Tanimoto et al., 2017). It was further found that the ASH response to a small odor increase is decreased by odor preexposure, indicating an experience-dependent modulation of its activity (Yamazaki et al., 2019).

ASH neurons are considered as a simple model for polymodal nociceptive neurons evolutionarily conserved from worms to mammals (Kaplan and Horvitz, 1993). Thus, analyzing the ASH response to 2-nonanone will be ideal to address questions below at the levels of behavior, neural activity, and molecules. For example, how do sensory neurons adapt their sensitivity for behavioral responses to ever-changing environmental stimuli, which cellular mechanisms support changes in response after experiencing a stimulus, and what is the molecular mechanism for its implementation.

Aim and approaches of this study

In this study, I aimed to elucidate the mechanism of modulation in response of sensory neurons. Therefore I investigated whether and how responses of ASH sensory neurons are

modulated during repulsive odor learning in *C. elegans*. Then I found that sensory gain control occurs in ASH sensory neurons for efficient odor avoidance by preexposure to 2-nonanone via specific suppression of one of its activity components.

Subjecting the animals to a series of gradual changes in odor concentration by using OSB2 revealed that preexposed ASH neurons became less sensitive to smaller increases in odor concentration, while their responses to larger increases did not change. In other words, preexposure changed the slope of the stimulus–response relationships, i.e. gain control. This experience-dependent modulation of sensory activity is consistent with the changes in the animals' behavioral responses: they respond less to small increases in odor concentration, likely leading to more efficient odor avoidance not disturbed by a noisy and/or fluctuating odor concentration change.

On modeling the ASH response mathematically, I found that the slow and fast components of ASH response were well fitted as the sum of the leaky integration of the first- and second-order time-differentials of odor concentration, respectively. Notably, the preexposure experience specifically suppressed only the fast component. Furthermore, genetic analysis suggested that G protein signaling may regulate the fast component after preexposure. Thus, these results demonstrate how experience-dependent modulation of stimulus–response relationships occurs and how it leads to changes in behavioral responses.

MATERIALS AND METHODS

Strains.

The techniques I used to culture and handle *C. elegans* were essentially as described previously (Brenner, 1974). *C. elegans* wild-type Bristol strain N2, JC2628 *osm-9(ky10) ocr-2(ak47)*, RB1780 *rgs-3(ok2288)*, MT1073 *egl-4(n478)*, DR1089 *unc-77(e625),* and VC550 *tag-180(ok779)*, were obtained from the Caenorhabditis Genetics Center (University of Minnesota, USA). In all the behavioral and physiological experiments, I used young adult hermaphrodites.

Calcium imaging by OSB2 system.

Calcium imaging of ASH sensory neurons was performed as previously reported (Tanimoto et al., 2017; Tanimoto and Kimura, 2021). In brief, transgenic lines expressing GCaMP3 (Tian et al., 2009) and mCherry (Shaner et al., 2004) in ASH (20 ng/µl of *sra-6p*::GCaMP3, 20 ng/µl of *sra-6p*::mCherry, 10 ng/µl of *lin-44p*::GFP, 50 ng/µl of PvuII-cut N2 genomic DNA) were placed on NGM plates and observed under the Kimura laboratory's original microscope system, OSB2. To measure the neural activity of multiple animals in a single observation, the transgenic animals were immobilized using levamisole, an agonist to the acetylcholine receptor (Lewis et al., 1980); ASH response is not affected by levamisole treatment (Tanimoto et al., 2017).

For odor stimulation, I delivered a mixture of 2-nonanone and air at a total of 8 mm/min and

created a temporal changing gradient of odor concentration by changing the ratio of 2-nonanone to air. I measured this gradient using a custom-made semiconductor sensor before and after performing the calcium imaging experiments on each day (Tanimoto and Kimura, 2021).

I divided the fluorescent signals of GCaMP3 and mCherry through a dual-wavelength measurement optical system, w-view (Hamamatsu Photonics), and captured their fluorescence images using an EM-CCD camera (ImagEM, Hamamatsu Photonics) at a sampling rate of 10 Hz. After subtracting the background, I extracted the fluorescence intensity of the cell body using ImageJ (NIH) and used their ratio (GCaMP/mCherry) as the data.

Conditioning of the animals.

Calcium imaging of ASH was performed using OSB2 under the following three conditions. (1) Naive: the animals were cultivated on 6 cm NGM plates with OP50 provided as food, and were then washed briefly with NGM buffer and measured; (2) Preexp: the animals were preexposed to 0.6 µl of 15% 2-nonanone (diluted in ethanol) for 1 hour on a 6 cm NGM plate without food; and (3) Mock-treated: the animals were preexposed to ethanol in the same way as the preexp condition. The mock-treated condition is a control that shows that starvation itself does not affect the response to 2-nonanone.

Data analysis and statistical analysis.

In the calcium imaging experiments, data were obtained two to three days in each condition. Experimental conditions, such as strains, odor stimuli and conditioning of the animals, were randomly set for each day. After the data acquisition, animals with too weak intensity of basal mCherry or GCaMP3 fluorescence for tracking were excluded. To exclude noise, frames in which the GCaMP/mCherry ratio was in the top 1% and bottom 1% of the total were removed. Statistical analyses were performed using the Kruskal-Wallis test with a *post-hoc* Steel-Dwass test using R (The R Project). In the figure, * indicates $p < 0.05$, ** indicates $p < 0.01$, and *** indicates $p < 0.001$. Scatter plots represent median ± quartiles and other graphs represent the mean ± standard error. I chose the sample size based on a large scale behavioral analysis of *C. elegans* (Yemini et al., 2013).

Mathematical modeling of AWB-like responses by leaky integration.

Mathematical modeling of AWB-like responses was described in a previous work in the Kimura laboratory (Tanimoto et al., 2017). In brief, the activity of AWB neurons, which responds to decreases in 2-nonanone concentration, is well fitted with the following leaky integrator equation:

$$\frac{dX(t)}{dt} = I - \frac{1}{\tau}(X(t) - X_e) \quad (1)$$

$$I = -k\frac{dC(t)}{dt}$$

where $X(t)$ is the measured fluorescence signal of the neuron (GCaMP/mCherry), I is the input, X_e is the basal calcium level in the steady state, k and $1/\tau$ are the parameters, and $C(t)$ is

the measured odor concentration. The model parameters k, $1/\tau$, and X_e were determined by the least-squares method (Excel solver). This Eq. (1) indicates that the neuronal response *X(t)* increases according to the input (negative *dC(t)/dt*) and reduces ("leaks") according to the *X(t)* itself and returns to the steady state X_e. For example, when an animal experiences a constant decrease in odor concentration (*e.g.*, Figure 3C), the constant decrease is transformed to a constant depolarization, and it causes constant calcium influx via L-type VGCC EGL-19, and the calcium concentration reduces according to its total amount possibly via leak channel(s) (Tanimoto et al., 2017). Since AWB neurons respond to decreases in odor concentration, zero is substituted to *dC(t)/dt* when *dC(t)/dt* is positive in Eq. (1). This AWB activity was essentially abolished by treatment of animals with Nemadipine-A (NemA), the antagonist of *C. elegans* L-type VGCC (Kwok et al., 2006), indicating that the AWB activity is mainly mediated by the L-type VGCC homolog EGL-19.

In NemA-treated animals, ASH neurons are rapidly activated at the beginning of the odor-increasing phase but soon inactivated gradually even though the odor concentration kept increasing (red dotted line in Figure 3D). When I assumed that the NemA-treatment suppressed AWB-like leaky integration activity (yellow dotted line in Figure 3D), the sum of the remaining and the suppressed activity (blue solid line in Figure 3D) nicely resembled the measured ASH activity (black solid line in Figure 3D). The transient and gradual activities are called the fast and slow components, respectively (Tanimoto et al., 2017).

The first and second differential model of ASH responses.

I extended the previous model Eq. (1) by introducing the second-order time differential of input *C* representing the fast component:

$$\frac{dX(t)}{dt} = k_1 \frac{dC(t)}{dt} + k_2 \frac{d^2C(t)}{dt^2} - \frac{1}{\tau}(X(t) - X_e) \quad (2)$$

where $X(t)$ is the measured ASH signal, X_e is the basal calcium level, and k_1, k_2 and $1/\tau$ are parameters for the first- and second-order time differential and leaky part, respectively. The parameters k_1, k_2, $1/\tau$, and X_e were determined by the least-squares method for each odor stimulus. $dC(t)/dt$ and $d^2C(t)/dt^2$ were calculated using the central difference scheme. Since ASH neurons respond to increases in odor concentration (Tanimoto et al., 2017), zero is substituted to $dC(t)/dt$ or $d^2C(t)/dt^2$ when $dC(t)/dt$ or $d^2C(t)/dt^2$ is negative in Eq. (2).

The first and second differential model Eq. (2) is further extended on the terms of the second-order time-differential and X_e:

$$\frac{dX(t)}{dt} = k_1 \frac{dC(t)}{dt} + \Phi\left(k_2 \frac{d^2C(t)}{dt^2}\right) - \frac{1}{\tau}\big(X(t) - X_e(t)\big), \quad (3)$$

where $\Phi(x)$ is the saturation function as the following equation:

$$\Phi(x) = \begin{cases} 0.14, if\ x > 0.14 \\ x\ , if\ \ x \leq 0.14 \end{cases} \quad (4)$$

This saturation function is introduced to prevent the parameters from becoming too large when the increase in odor concentration approaches zero. 0.14 was arbitrary determined. $X_e(t)$ changes over time as follows:

$$X_e(t) = \begin{cases} b_1 & ,if\ t < t_1 \\ \dfrac{b_2 - b_1}{t_2 - t_1} t + \dfrac{t_2 b_1 - t_1 b_2}{t_2 - t_1} & ,if\ t_1 \le t \le t_2 \\ b_2 & ,if\ t_2 < t \end{cases} \quad (5)$$

where t_1 is the time at the start of the first odor increase phase, and t_2 is the time at the end of the first odor increase phase. The parameters b_1 and b_2 were determined by the least-squares method with the actual ASH response during 30 seconds until 10 seconds before the start of the first odor increase phase (t_1) and 1 minute after the first odor stimulus (t_2), respectively. Eq. (5) was introduced because the basal calcium level changed after the first odor stimulus.

In terms of parameters in Eq. (3), I plotted the relationships among parameters (k_1, k_2, and $1/\tau$) and various aspects of odor inputs (average, maximum, or accumulation of C, dC/dt, and d^2C/dt^2) and fitted the relationships to the logarithmic function ($y = f \ln(x) + g$) of the odor inputs (Excel solver); fitting of k_1 and $1/\tau$ to linear functions ($y = h\ x + i$) of the odor inputs was worsened (Table 1). I chose the aspect of odor input with the smallest or the second smallest residual sum of squares, and the logarithmic function of my chosen aspect for k_1 and $1/\tau$ were similar between naive, mock-treated and preexposed conditions. Thus I further optimized f and g manually such that they were the same for all three conditions.

As a lower threshold for $1/\tau$, the following function is introduced:

$$\frac{1}{\tau} = \begin{cases} 0.02\ ln(x) + 0.11, if\ x > 0.1 \\ 0.02\ ln(0.1) + 0.11, if\ x \le 0.1 \end{cases} \quad (6)$$

where x denotes $d^2C(t)/dt^2$. This function is introduced to prevent $1/\tau$ from becoming too small when the increase in odor concentration approaches zero. 0.1 was arbitrary determined.

Evaluation of the mathematical model.

The Bayesian information criterion (BIC) (Schwarz, 1978) was used to assess the fit of the data using a mathematical model. The smaller the BIC value, the better is the model fit. In BIC, the goodness of fit for the model, including a penalty term to prevent overfitting, is given by the following equation:

$$\mathrm{BIC} = Nln\left(\frac{RSS}{N}\right) + Mln(N) \tag{7}$$

where N is the number of frames used for the fitting, RSS is the sum of the squared residuals between the model and the actual response, and M is the number of free parameters used in the model. M=2 for the original simple time-differential model because of k and X_e, M=3 for the model with the leaky integration of only first- or second-order time-differential because of k_1 or k_2 and $1/\tau$ and X_e, M=4 for the first and second differential model because of k_1, k_2, $1/\tau$ and X_e, and M=12 for the first and second differential model with stimulus-dependent parameters because there were two parameters each in the stimulus-dependent parameters k_1, k_2, and $1/\tau$, four parameters in $X_e(t)$, one parameter in $\Phi(x)$, and one parameter in lower threshold for $1/\tau$.

Behavioral analysis.

Trajectories obtained by a high-resolution USB camera (DMK72AUC02; The Imaging

Source, United States) during 2-nonanone avoidance behavior were clustered using the previously reported STEFTER method (Yamazaki et al., 2019). In brief, clustering was performed using variances of temporal changes in bearing, and the cluster with the smallest variances of temporal changes in bearing was classified as “run”, while the other clusters were classified as “pirouette” categories. This classification of “run” and ”pirouette” was more than 90% consistent with the previous one based on the durations of straight migration (Yamazoe-Umemoto et al., 2015). Then, the change in the odor concentration sensed during the run was calculated according to an odor gradient model based on the measured odor concentrations (Yamazoe-Umemoto et al., 2015). The behavioral data used in this study have already been analyzed and published previously (Yamazaki et al., 2019).

RESULTS

Sensory gain control in ASH neurons caused by odor preexposure.

To reveal how experience changes the activities of sensory neurons under conditions of physiologically meaningful odor stimuli, I investigated ASH activities before and after preexposure to 2-nonanone. Previous quantitative behavioral analysis in the Kimura laboratory revealed that *C. elegans* senses approximately 5–20 nM/s concentration changes during 2-nonanone avoidance behavior (Yamazoe-Umemoto et al., 2015). Therefore, in this experiment, I used three types of stimuli in a series of odor stimulations (odor gradient #2): (1) a minimum increase that could be provided stably by the Kimura laboratory's original microscope system OSB2 (3 nM/s) (Tanimoto et al., 2017); (2) a maximum increase sensed during the behavioral experiment (20 nM/s); and (3) an even larger increase (40 nM/s). I measured the ASH response to these stimuli under three different conditions with prior treatments: naive, mock-treated, and preexposed (Figure 2).

In the naive condition, the ASH response to 3 nM/s started to increase immediately after the onset of odor increase, quickly reached close to the maximum value, and the magnitude of the response was sustained during the odor increase (Figure 4A). When the odor began to decrease, the response also decreased, and when the odor concentration returned to zero, the ASH response returned to a basal level. The ASH responses to 20 nM/s and 40 nM/s odor increases were essentially similar to the response to 3 nM/s in magnitude and pattern. The results of the mock-treated condition were similar to those of the naive animals. In summary,

the magnitude of the response was always constant in naive and mock-treated conditions, regardless of the magnitude of the odor increase.

In the preexposed condition, unlike naive and mock-treated animals, ASH did not respond much to the 3 nM/s increase: its maximum value was substantially smaller than those in the naive and the mock-treated animals, and the activity slowly increased and reached the maximum value at the end of the odor-increasing phase (Figure 4A). However, ASH responded strongly to the 20 and 40 nM/s increases, and the magnitude of the response increased according to the magnitude of the odor increase.

In terms of the maximum response to each odor increase, there was no significant difference in the responses to 20 and 40 nM/s, but the response to 3 nM/s was significantly smaller in the preexposed animals than in the naive and mock-treated animals (Figure 4B). The linear approximation of the average responses to each odor increase did not change much in the naive and mock-treated conditions, but was positive in the preexposed condition (Figure 4C). Furthermore, by calculating the slope of each animal's response to the 3, 20, and 40 nM/s stimuli, I found that the slopes of the preexposed response were significantly larger than those of the naive and mock-treated responses (Figure 4D). Thus, the slope of stimulus–response relationships of ASH neurons changes because of preexposure to the odor, not adaptation or sensitization, which is an overall increase or decrease of the relationships without changes in its slope (Figure 1). In other words, gain control occurs in ASH neurons because of

preexposure to the odor.

This gain control in ASH neurons is consistent with the result of behavioral analysis performed by my colleague Dr. Yamazaki. The analysis of the correlations between odor concentration changes and behavioral aspects of the animals revealed that the change in odor concentration upon initiation of the pirouette phase was almost zero in the naive and mock-treated conditions, but was positive in the preexposed condition (Figure 4E). This suggests that naive and mock-treated animals initiate pirouettes in response to very small increases in odor concentration, while the preexposed animals respond only to larger increases. According to this result and ASH gain control, the enhanced odor avoidance behavior by the animals after odor preexposure can be explained (Figure 5) (see Discussion).

Modeling the experience-dependent gain control in ASH activity.

In order to obtain quantitative insights into the mechanism of gain control caused by preexposure, I performed mathematical modeling of the ASH response. In previous study, the ASH response to the simple gradual odor increase (odor gradient #1) was modeled by simple time-differential of odor concentration (Tanimoto et al., 2017). Furthermore, pharmacological study suggested the ASH response to the odor gradient #1 consists of fast and slow components (Figure 3D). The slow component was modeled by the leaky integration of time-differential (dC/dt) of odor concentration (C) like the AWB response (Figure 3C). However, the simple time-differential model and the leaky integration of time-differential model

(Equation 1 in Materials and Methods) did not reproduce the ASH responses sufficiently, especially the fast component of the naive and mock-treated ASH responses to the odor gradient #2 (Figure 6 and 7).

Next, I modeled the fast component of ASH response mathematically. The fast component started to increase at the onset of odor concentration increase, and soon it started to decrease even when the odor concentration continued to increase (red dotted line in Figure 3D). This time course of the fast component can be approximated by a leaky integration of the second-order time-differential (d^2C/dt^2) of the odor concentration (vertical gray bar and red line in "d^2C/dt^2" panel in Figure 8A). To this end, I extended the model, hereafter referred to as "first and second differential model", where the ASH response itself is represented by a leaky integration of the sum of both the first- and second-order time-differentials of the odor concentration (Figure 8A; Equation 2 in Materials and Methods).

I examined whether the first and second differential model could reproduce the ASH responses to odor gradients #1 and #2. By determining the model parameters to the odor gradient #1 and each odor stimulus in odor gradient #2 independently, in most of the conditions the model reproduced the ASH activities well, including the fast component (blue lines in Figure 8B). I should note that the contribution of the fast component in ASH activities was significantly lower in preexposed than in naive and mock-treated conditions (red lines in right panels in Figure 8B), indicating that the fast component was specifically

suppressed by the preexposure (see below).

To test the optimality of the first and second differential model, I compared the goodness of fit among the first and second differential model and three other models: the original simple time-differential model, and leaky integration of only first- or second-order time-differential models (Figure 6, 7 and 9, respectively). By calculating the Bayesian Information Criterion (BIC) (Schwarz, 1978) for each model, I found that the first and second differential model had the best or close-to-the-best goodness of fit in all naive and mock-treated conditions (Table 2), demonstrating the optimality of the model for these conditions. In the preexposed condition, the leaky integration of first-order time-differential model had the best fit, consistently with the suppression of the fast (second-order time-differential) component in ASH activity (Figure 8B right).

The contribution of the first and second differential exhibited a remarkable difference for every odor gradient #2 (Figure 8B right). For example, in naive and mock-treated conditions, the fast component became smaller when odor concentration increased more rapidly (compare the response to the 3 nM/s increase to the ones to the 20 and 40 nM/s increases). Consistently, when these parameters were uniquely determined for all the odor stimuli, the model did not accurately reproduce the ASH responses to odor gradient #2 (Figure 10). These results suggest that the parameters depend on some aspects of the stimuli such as the odor concentration and/or its changing velocity.

To test whether and how the parameters depend on aspects of stimuli, I plotted the relationships between the parameters and multiple aspects of the odor stimuli. I found that each parameter approximately follows a logarithmic function of the stimulus intensity (Figure 11). Interestingly, in the well-fitted cases (red rectangles in Figure 11), this function of the slow component (k_1) and the leaky part ($1/\tau$) were similar among naive, mock-treated and preexposed conditions, although that of the fast component (k_2) was much lower for preexposed than for naive and mock-treated conditions. When I further introduced this stimulus intensity dependency into the first and second differential model (Equation 3 in Materials and Methods), the model unifyingly reproduced the ASH responses to odor gradients #1 and #2 as well as their gain control-dependent changes (Figure 12A and B). These results suggest that the contributions of fast and slow components and the leak of ASH response depend on the logarithmic function of the odor stimulus intensity and that the fast component is further suppressed after odor preexposure for the gain control. The differences in the relationships between stimuli aspects and each parameter may reflect the regulatory mechanisms of fast and slow components and the leak activity (see Discussion).

Genetic analysis of the ASH response.

Finally, I tried to identify the genes responsible for the fast component of ASH responses. Specifically I looked for mutants that exhibit the slow component-like response in naive or mock-treated (*i.e.*, control) conditions.

I first analyzed mutants of cation channels. *osm-9* and *ocr-2* are the homologs of TRPV cation channels and known to function in ASH neurons for depolarization caused by sensory stimuli (Colbert et al., 1997; Tobin et al., 2002) although their physiological role in 2-nonanone sensation has not been revealed. *osm-9 ocr-2* double mutants exhibited substantially no response (Figure 13A), suggesting that they are also required for sensory depolarization caused by 2-nonanone. The L-type VGCC subunit α1 EGL-19 is responsible for the slow component, although loss-of-function mutations in N- and T- types of VGCC subunit α1, *unc-2* and *cca-1* respectively, did not affect ASH response to the odor (Tanimoto et al., 2017). In this study I tested the homologs of a VGCC auxiliary subunit α2δ2 and a sodium leak channel, *tag-180* and *unc-77*, respectively (Lainé et al., 2011; Yeh et al., 2008). Both of the mutant strains exhibited wild-type like responses that were properly fitted with the ASH model (Figure 13A), indicating that these genes are not involved in the ASH response either.

I then analyzed other candidates that have been known to be involved in modulation of sensory neuronal activity in *C. elegans*: *egl-4* (cyclic GMP-dependent protein kinase: PKG), and *rgs-3* (regulator of G protein signaling: RGS) (Ferkey et al., 2007; L'Etoile et al., 2002). The ASH responses of *egl-4* and *rgs-3* mutants in the control condition were substantially suppressed (black lines in Figure 13A). Remarkably, the ASH responses of *egl-4* and *rgs-3* mutants were best fitted with the first-order (*i.e.*, slow) only model (yellow lines in Figure 13A and Table 3), suggesting that the fast component of ASH activity requires these gene

products. It has been reported that EGL-4 phosphorylates RGS-3, and loss-of-function mutations in either of the genes increases ASH neuronal and ASH-mediated behavioral responses to other repulsive stimuli (Krzyzanowski et al., 2013). Therefore, this PKG–RGS pathway may regulate the fast component of the ASH response in a different manner from this previous report (see Discussion).

DISCUSSION

2-nonanone avoidance enhancement by gain control in ASH sensory neurons.

In this study, I demonstrated that the responsiveness of the ASH sensory neurons of *C. elegans* to 2-nonanone exhibits gain control after preexposure to the odor. In naive and mock-treated conditions, ASH always exhibits a large response regardless of the rate of odor increase, whereas in the preexposed condition, the response to a small gradual increase became smaller and the response to a large gradual increase remains unchanged (Figure 4A-D). This suggests that gain control to change the slope of stimulus–response relationships is caused by experiencing odor preexposure.

Based on previous findings (Tanimoto et al., 2017) and the results of this study (Figure 4E), I consider that this sensory gain control contributes to the ability of *C. elegans* to efficiently navigate down the gradient of repulsive odor. The animals in the 2-nonanone avoidance assay generally move away from the odor source and sense decreases in the odor concentration. However, their movements away from the odor source are frequently interrupted because of stochastic occurrence of pirouettes and/or of small increases in odor concentration (Yamazoe-Umemoto et al., 2015). This increase of odor concentration could be caused by (1) the direction of the animals' movement straying from the ideal, (2) small fluctuations in the odor gradient, and/or (3) small periodic changes in the sensed odor concentration caused by the animals' sinusoidal head swing. In the naive and mock-treated conditions, the animals initiate pirouettes when they experience even a small increase in odor concentration (Figure 5, top

left). However, in the preexposed condition, the animals do not respond to small increases (Figure 5, top right), which results in a longer avoidance distance traveled in the same period. They still initiate pirouettes when they sense larger increases (Figure 5, bottom panels). Thus, experience-dependent changes in ASH response due to gain control likely contribute the enhanced odor avoidance behavior, which could also be effective in a real-world environment infused with noise.

To my knowledge, this is the first report of sensory gain control in wild-type *C. elegans*. There are multiple examples of behavioral changes in *C. elegans* due to activity changes in sensory neurons that are affected by repeated stimuli, different types of stimuli, or the feeding state (Chew et al., 2018; Ezcurra et al., 2016; Larsch et al., 2015). However, most of the response changes in wild-type animals are caused by adaptation or sensitization but not gain control. It is possible that the animals might have developed a special mechanism against this odorant to effectively avoid danger because it is one of the two major volatile compounds produced by *P. aeruginosa*, a bacterial species that is pathogenic to *C. elegans* (Labows et al., 1980; Tan et al., 1999; Tan and Ausubel, 2000).

Estimating the neural mechanism of gain control by mathematical modeling.

To obtain quantitative insights into the mechanism of sensory gain control, I performed mathematical modeling. Indeed, mathematical modeling has successfully revealed essential features of the sensory neuronal responses of the animals (Ikeda et al., 2021; Itskovits et al.,

2018; Kato et al., 2014; Tanimoto et al., 2017). Previous pharmacological analysis in the Kimura laboratory revealed that ASH activity is composed of fast and slow components, and I showed in this study that the fast component can be approximated by a leaky integration of the second-order time-differential of the odor concentration (Figure 8). Even independent of the pharmacological result, the ASH responses in wild-type animals exhibit overshoot in response to a long-lasting and linearly increasing odor concentration (odor gradient #1 in Figure 3D and Figure 8B, and odor gradient #3 in Figure 13A). More precisely, the response first increases rapidly, and then slowly decreases to a non-zero constant value. The leaky integration of the first-order time-differential of the odor concentration generates a sustained response that converges to a non-zero constant value. The leaky integration of the second-order time-differential generates a rapidly increasing and subsequently decreasing response. Thus, both the pharmacological analysis as well as the analysis of shapes of ASH response in time domain suggest that the ASH response can be modeled with a leaky integration of the sum of the first- and second-order time-differentials of the odor concentration, and that these two terms well describe essential characteristics of ASH neurons. Indeed, the model had the best goodness of fit in most naive and mock-treated conditions in terms of BIC (Table 2). It should be noted, however, that I only tested the leaky integration of the second-order time-differential equation to the constantly increasing odor gradients, and the equation may not be applicable to ASH responses to other types of odor stimuli; in other words, the fast component could be approximated with another equation such as an alpha function (Rall, 1967). However, since this alpha function ($f(t) = F_{Max}\frac{t}{\tau}e^{-\frac{t}{\tau}}$) is expressed only in terms of

the maximum value (F_{Max}) and leak speed (τ), it does not reflect how the stimulus is affected to ASH, and it does not understand what the cellular mechanism related. The leaky integration of the sum of the first- and second-order time-differential equation with stimulus-dependent parameters nicely reproduced the ASH responses, and provided us an important biological insight (see next section). Some details still do not match, suggesting the involvement of other factors in the ASH response.

Remarkably, my mathematical model indicates that the preexposure-dependent changes in ASH response can be caused only by the modulation of the fast component (k_2) rather than the modulation of overall ASH response, although the ASH response does exhibit changes in multiple aspects, such as its speed, magnitude, and small increase/decrease when it reaches closes to the maximum value (odor gradient #2 in Figure 8B). It also explains why ASH responses to a large odor increase are not substantially affected. This result suggests that a specific sensory signaling molecular pathway that suppresses the fast component in ASH neurons is regulated by preexposure to cause experience-dependent modulation of behavior, *i.e.*, learning.

Relationships between the mathematical model and molecular mechanisms of ASH response.

The Kimura laboratory has previously shown that AWB responses are mediated by EGL-19, an α1 subunit of L-type VGCC, which possesses a long-lasting channel opening property, and

that a $G\alpha_o$ homolog, GOA-1, is required for the first-order time-differential of odor concentration (Tanimoto et al., 2017). These results suggest that the constant decrease in 2-nonanone concentration is time-differentiated at the sensory ending by G protein signaling and causes constant depolarization, leading to EGL-19 opening and a continuous influx of calcium into the cells. The slow component in ASH neurons is also mediated by EGL-19 (Bargmann, 2006; Tanimoto et al., 2017).

In contrast, the fast component in ASH neurons is likely caused by a transient calcium influx at the onset of odor concentration increase, which ends rapidly (Figures 8A and 13B left). One candidate gene product for this was the T-type VGCC ("T" for transient opening) (Nowycky et al., 1985). However, the loss-of-function mutant of the *cca-1* gene, the sole homolog of T-type VGCC in *C. elegans* (Steger et al., 2005), showed wild-type-like ASH responses (Tanimoto et al., 2017). In addition, the loss-of-function mutants of N-type homolog *unc-2* (Tanimoto et al., 2017) and of the homologs of VGCC auxiliary subunit α2δ2 *tag-180* (Figure 13A) also exhibited a wild-type-like response, suggesting that some other calcium channel(s) may be involved in the fast component.

Still, I found that PKG EGL-4 and RGS RGS-3 possibly modulate the fast component. RGS is known to inhibit G protein signaling to modulate the magnitude and/or time-course of neuronal responses in *C. elegans* and mammals (Cao et al., 2012; Krzyzanowski et al., 2013; Lur and Higley, 2015). In addition, PKG phosphorylates RGS to increase its activity in *C.*

elegans and mammals (Huang et al., 2007; Krzyzanowski et al., 2013). Because the effects of PKG–RGS activation on neuronal responses are different from the previous report in which this pathway activated the ASH response to other stimulus (Krzyzanowski et al., 2013), I consider that these gene products may inhibit G protein activity which suppresses the ASH response. In other words, in naive/mock-treated ASH neurons, the PKG–RGS pathway inhibits G protein activity that suppresses the ion channel that mediates the fast component, and preexposure suppresses the PKG–RGS pathway, leading to activation of G protein and to inhibition of the fast component (Figure 13B).

While genetic analysis itself is static (*i.e.*, it would not provide me information related to time-course changes of the gene product activities), the combination with physiological analysis and mathematical modeling provides insights as to how these gene products affect neural activities dynamically. For example, the characteristics of ASH neurons in wild-type animals are not clear except for the preexposure-dependent gain control aspect, although a simple "first and second differential model" can explain multiple aspects of the differences, such as the quick rise at the onset of the odor stimulus, the gradual decrease during a long-lasting odor increase, the slow decay during odor decrease (not reproduced by the original simple time-differential model) as well as the gain control (Figures 8 and 12B). Furthermore, the stimulus-dependent parameters I used in the model may reflect the opening probabilities of the channels for the fast and slow responses, which change according to the intensity of the stimulus. For example, k_1 reduces according to the accumulation of odor concentration

(Figure 12A), which may indicate habituation due to the sustained stimulation from the odor. Further, k_2 reduces according to the average of dC/dt, suggesting that the depolarization level may affect the opening probability because the odor concentration is time-differentiated at the sensory ending and it reflects the depolarization level (Tanimoto et al., 2017). Lastly, $1/\tau$ increases according to the second-order time-differential of odor concentration, which may reflect a change in leakage level at the stimulus onset. Those insights could have not been obtained without the model.

In summary, my results demonstrate that gain control occurs in ASH sensory neurons after preexposure to the repulsive odor, and mathematical analysis suggests that this gain control is caused by suppression of the fast component, which could be caused by transient cation influx at the onset of odor concentration increase. This gain control leads to efficient avoidance behavior that allows the animal to ignore slight increases in odor concentration while moving down the odor gradient, thereby enhancing the avoidance distance. In more complex animals, such as mice and *Drosophila*, neurotransmitters such as serotonin or GABA are involved in gain control in peripheral and central sensory systems (Azimi et al., 2020; Olsen and Wilson, 2008) but it is not clear about what molecules are involved in the cellular mechanism, how their functions are modulated in gain control, and how the sensory gain control affects behavioral change. My study may contribute to our understanding of intracellular mechanisms surrounding sensory gain control and its effects for behavior in animals.

REFERENCE

Andersen RA, Essick GK, Siegel RM. 1985. Encoding of spatial location by posterior parietal neurons. *Science* **230**:456–458. doi:10.1126/science.4048942.

Anderson CT, Kumar M, Xiong S, Tzounopoulos T. 2017. Cell-specific gain modulation by synaptically released zinc in cortical circuits of audition. *Elife* **6**:1–20. doi:10.7554/eLife.29893

Azimi Z, Barzan R, Spoida K, Surdin T, Wollenweber P, Mark MD, Herlitze S, Jancke D. 2020. Separable gain control of ongoing and evoked activity in the visual cortex by serotonergic input. *Elife* **9**:1–29. doi:10.7554/eLife.53552

Bargmann CI. 2006. Chemosensation in C. elegans. *WormBook* 1–29. doi:10.1895/wormbook.1.123.1

Bargmann CI, Hartwieg E, Horvitz HR. 1993. Odorant-selective genes and neurons mediate olfaction in C. elegans. *Cell* **74**:515–527. doi:10.1016/0092-8674(93)80053-H

Brenner S. 1974. The genetics of Caenorhabditis elegans. *Genetics* **77**:71–94. doi:10.1093/genetics/77.1.71.

Cao Y, Pahlberg J, Sarria I, Kamasawa N, Sampath AP, Martemyanov KA. 2012. Regulators of G protein signaling RGS7 and RGS11 determine the onset of the light response in on bipolar neurons. *Proc Natl Acad Sci U S A* **109**:7905–7910. doi:10.1073/pnas.1202332109

Carew TJ, Castellucci VF, Kandel ER. 1971. An analysis of dishabituation and sensitization

of the gill-withdrawal reflex in aplysia. *Int J Neurosci* **2**:79–98. doi:10.3109/00207457109146995

Castellucci V, Pinsker H, Kupfermann I, Kandel E. 1970. Neuronal mechanisms of habituation and dishabituation of the gill-withdrawal reflex in Aplysia. *Science* **167**:1745–1748. doi:10.1126/science.167.3926.1745

Chance FS, Abbott LF, Reyes AD. 2002. Gain modulation from background synaptic input. *Neuron* **35**:773–782. doi:10.1016/S0896-6273(02)00820-6

Chew YL, Tanizawa Y, Cho Y, Zhao B, Yu AJ, Ardiel EL, Rabinowitch I, Bai J, Rankin CH, Lu H, Beets I, Schafer WR. 2018. An Afferent Neuropeptide System Transmits Mechanosensory Signals Triggering Sensitization and Arousal in C. elegans. *Neuron* **99**:1233-1246.e6. doi:10.1016/j.neuron.2018.08.003

Colbert HA, Smith TL, Bargmann CI. 1997. OSM-9, a novel protein with structural similarity to channels, is required for olfaction, mechanosensation, and olfactory adaptation in Caenorhabditis elegans. *J Neurosci* **17**:8259–8269. doi:10.1523/jneurosci.17-21-08259.1997

De Bono M, Maricq AV. 2005. Neuronal substrates of complex behaviors in C. elegans. *Annu Rev Neurosci* **28**:451–501. doi:10.1146/annurev.neuro.27.070203.144259

Dragoi V, Sharma J, Sur M. 2000. Adaptation-induced plasticity of orientation tuning in adult visual cortex. *Neuron* **28**:287–298. doi:10.1016/S0896-6273(00)00103-3

Ebrey T, Koutalos Y. 2001. Vertebrate Photoreceptors. *Prog Retin Eye Res* **20**:49–94. doi:10.1016/S1350-9462(00)00014-8

Ezcurra M, Walker DS, Beets I, Swoboda P, Schafer WR. 2016. Neuropeptidergic signaling and active feeding state inhibit nociception in Caenorhabditis elegans. *J Neurosci* **36**:3157–3169. doi:10.1523/JNEUROSCI.1128-15.2016

Ferkey DM, Hyde R, Haspel G, Dionne HM, Hess HA, Suzuki H, Schafer WR, Koelle MR, Hart AC. 2007. C. elegans G Protein Regulator RGS-3 Controls Sensitivity to Sensory Stimuli. *Neuron* **53**:39–52. doi:10.1016/j.neuron.2006.11.015

Ferkey DM, Sengupta P, L'Etoile ND. 2021. Chemosensory signal transduction in Caenorhabditis elegans. *Genetics* **217**. doi:10.1093/GENETICS/IYAB004

Hilliard MA, Apicella AJ, Kerr R, Suzuki H, Bazzicalupo P, Schafer WR. 2005. In vivo imaging of C. elegans ASH neurons: Cellular response and adaptation to chemical repellents. *EMBO J* **24**:63–72. doi:10.1038/sj.emboj.7600493

Huang J, Zhou H, Mahavadi S, Sriwai W, Murthy KS. 2007. Inhibition of Gαq-dependent PLC-β1 activity by PKG and PKA is mediated by phosphorylation of RGS4 and GRK2. *Am J Physiol - Cell Physiol* **292**:200–208. doi:10.1152/ajpcell.00103.2006

Ikeda M, Matsumoto H, Izquierdo EJ. 2021. Persistent thermal input controls steering behavior in Caenorhabditis elegans. *PLoS Comput Biol* **17**. doi:10.1371/JOURNAL.PCBI.1007916

Itskovits E, Ruach R, Kazakov A, Zaslaver A. 2018. Concerted pulsatile and graded neural dynamics enables efficient chemotaxis in C. elegans. *Nat Commun* **9**. doi:10.1038/s41467-018-05151-2

Kandel E. 2001. The molecular biology of memory storage : A dialogue between genes and

synapses. *Science* **294**:1030–1038. doi:10.1126/science.1067020.

Kaplan JM, Horvitz HR. 1993. A dual mechanosensory and chemosensory neuron in Caenorhabditis elegans. *Proc Natl Acad Sci U S A* **90**:2227–2231. doi:10.1073/pnas.90.6.2227

Kato S, Xu Y, Cho CE, Abbott LF, Bargmann CI. 2014. Temporal Responses of C.elegans Chemosensory Neurons Are Preserved in Behavioral Dynamics. *Neuron* **81**:616–628. doi:10.1016/j.neuron.2013.11.020

Kimura KD, Fujita K, Katsura I. 2010. Enhancement of odor avoidance regulated by dopamine signaling in Caenorhabditis elegans. *J Neurosci* **30**:16365–16375. doi:10.1523/JNEUROSCI.6023-09.2010

Krzyzanowski MC, Brueggemann C, Ezak MJ, Wood JF, Michaels KL, Jackson CA, Juang BT, Collins KD, Yu MC, L'Etoile ND, Ferkey DM. 2013. The C. elegans cGMP-Dependent Protein Kinase EGL-4 Regulates Nociceptive Behavioral Sensitivity. *PLoS Genet* **9**. doi:10.1371/journal.pgen.1003619

Kuhara A, Inada H, Katsura I, Mori I. 2002. Negative regulation and gain control of sensory neurons by the C. elegans calcineurin TAX-6. *Neuron* **33**:751–763. doi:10.1016/S0896-6273(02)00607-4

Kupfermann I, Castellucci V, Pinsker H, Kandel E. 1970. Neuronal correlates of habituation and dishabituation of the gill-withdrawal reflex in Aplysia. *Science* **167**:1743–1745. doi:10.1126/science.167.3926.1743

Kwok TCY, Ricker N, Fraser R, Chan AW, Burns A, Stanley EF, McCourt P, Cutler SR, Roy

PJ. 2006. A small-molecule screen in C. elegans yields a new calcium channel antagonist. *Nature* **441**:91–95. doi:10.1038/nature04657

L'Etoile ND, Coburn CM, Eastham J, Kistler A, Gallegos G, Bargmann CI. 2002. The cyclic GMP-dependent protein kinase EGL-4 regulates olfactory adaptation in C. elegans. *Neuron* **36**:1079–1089. doi:10.1016/S0896-6273(02)01066-8

Labows JN, McGinley KJ, Webster GF, Leyden JJ. 1980. Headspace analysis of volatile metabolites of Pseudomonas aeruginosa and related species by gas chromatography-mass spectrometry. *J Clin Microbiol* **12**:521–526. doi:10.1128/jcm.12.4.521-526.1980

Lainé V, Frøkjær-Jensen C, Couchoux H, Jospin M. 2011. The α1 subunit EGL-19, the α2/δ subunit UNC-36, and the β subunit CCB-1 underlie voltage-dependent calcium currents in Caenorhabditis elegans striated muscle. *J Biol Chem* **286**:36180–36187. doi:10.1074/jbc.M111.256149

Lamb TD, Pugh EN. 2004. Dark adaptation and the retinoid cycle of vision. *Prog Retin Eye Res* **23**:307–380. doi:10.1016/j.preteyeres.2004.03.001

Larsch J, Flavell SW, Liu Q, Gordus A, Albrecht DR, Bargmann CI. 2015. A Circuit for Gradient Climbing in C. elegans Chemotaxis. *Cell Rep* **12**:1748–1760. doi:10.1016/j.celrep.2015.08.032

Larsch J, Ventimiglia D, Bargmann CI, Albrecht DR. 2013. High-throughput imaging of neuronal activity in Caenorhabditis elegans. *Proc Natl Acad Sci U S A* **110**. doi:10.1073/pnas.1318325110

Lewis JA, Wu CH, Berg H, Levine JH. 1980. The genetics of levamisole resistance in the

nematode Caenorhabditis elegans. *Genetics* **95**:905–928. doi:10.1093/genetics/95.4.905

Lur G, Higley MJ. 2015. Glutamate Receptor Modulation Is Restricted to Synaptic Microdomains. *Cell Rep* **12**:326–334. doi:10.1016/j.celrep.2015.06.029

Nowycky MC, Fox AP, Tsien RW. 1985. Three types of neuronal calcium channel with different calcium agonist sensitivity. *Nature* **316**:440–3. doi:10.1038/316440a0

Ohzawa I, Sclar G, Freeman RD. 1982. Contrast gain control in the cat visual cortex. *Nature* **298**:266–268. doi:10.1038/298266a0

Olsen SR, Wilson RI. 2008. Lateral presynaptic inhibition mediates gain control in an olfactory circuit. *Nature* **452**:956–960. doi:10.1038/nature06864

Pierce-Shimomura JT, Morse TM, Lockery SR. 1999. The fundamental role of pirouettes in Caenorhabditis elegans chemotaxis. *J Neurosci* **19**:9557–9569. doi:10.1523/jneurosci.19-21-09557.1999

Pinsker H, Kupfermann I, Castellucci V, Kandel E. 1970. Habituation and dishabituation of the gill-withdrawal reflex in Aplysia. *Science* **167**:1740–1742. doi:10.1126/science.167.3926.1740

Priebe NJ, Ferster D. 2002. A new mechanism for neuronal gain control (or how the gain in brains has mainly been explained). *Neuron* **35**:602–604. doi:10.1016/S0896-6273(02)00829-2

Rall W. 1967. Distinguishing Theoretical Synaptic Potentials Computed for Different Soma-Dendritic Distributions of Synaptic. *J Neurophysiol* **5**:1138–68.

doi:10.1152/jn.1967.30.5.1138

Root CM, Masuyama K, Green DS, Enell LE, Nässel DR, Lee CH, Wang JW. 2008. A Presynaptic Gain Control Mechanism Fine-Tunes Olfactory Behavior. *Neuron* **59**:311–321. doi:10.1016/j.neuron.2008.07.003

Saro G, Lia AS, Thapliyal S, Marques F, Busch KE, Glauser DA. 2020. Specific Ion Channels Control Sensory Gain, Sensitivity, and Kinetics in a Tonic Thermonociceptor. *Cell Rep* **30**:397-408.e4. doi:10.1016/j.celrep.2019.12.029

Sasakura H, Mori I. 2013. Behavioral plasticity, learning, and memory in C. elegans. *Curr Opin Neurobiol* **23**:92–99. doi:10.1016/j.conb.2012.09.005

Schwarz G. 1978. Estimating the dimension of a model. *Ann Stat* **6**:461–464. doi:10.1214/aos/1176344136

Sengupta P, Chou JH, Bargmann CI. 1996. odr-10 Encodes a seven transmembrane domain olfactory receptor required for responses to the odorant diacetyl. *Cell* **84**:899–909. doi:10.1016/S0092-8674(00)81068-5

Shaner NC, Campbell RE, Steinbach PA, Giepmans BNG, Palmer AE, Tsien RY. 2004. Improved monomeric red, orange and yellow fluorescent proteins derived from Discosoma sp. red fluorescent protein. *Nat Biotechnol* **22**:1567–1572. doi:10.1038/nbt1037

Shapley R, Enroth-Cugell C. 1984. Visual Adaptation and Retinal Gain Controls. *Eng Sci* **3**:263–346. doi:10.1016/0278-4327(84)90011-7.

Steger KA, Shtonda BB, Thacker C, Snutch TP, Avery L. 2005. The C. elegans T-type calcium channel CCA-1 boosts neuromuscular transmission. *J Exp Biol* **208**:2191–2203. doi:10.1242/jeb.01616

Tan MW, Ausubel FM. 2000. Caenorhabditis elegans: A model genetic host to study Pseudomonas aeruginosa pathogenesis. *Curr Opin Microbiol* **3**:29–34. doi:10.1016/S1369-5274(99)00047-8

Tan MW, Mahajan-Miklos S, Ausubel FM. 1999. Killing of Caenorhabditis elegans by Pseudomonas aeruginosa used to model mammalian bacterial pathogenesis. *Proc Natl Acad Sci U S A* **96**:715–720. doi:10.1073/pnas.96.2.715

Tanimoto Y, Kimura KD. 2021. Calcium Imaging of Neuronal Activity under Gradually Changing Odor Stimulation in Caenorhabditis elegans. *Bio-Protocol* **11**:1–23. doi:10.21769/bioprotoc.3866

Tanimoto Y, Yamazoe-Umemoto A, Fujita K, Kawazoe Y, Miyanishi Y, Yamazaki SJ, Fei X, Busch KE, Gengyo-Ando K, Nakai J, Iino Y, Iwasaki Y, Hashimoto K, Kimura KD. 2017. Calcium dynamics regulating the timing of decision-making in C. Elegans. *Elife* **6**:1–30. doi:10.7554/eLife.21629

Tian L, Hires SA, Mao T, Huber D, Chiappe ME, Chalasani SH, Petreanu L, Akerboom J, McKinney SA, Schreiter ER, Bargmann CI, Jayaraman V, Svoboda K, Looger LL. 2009. Imaging neural activity in worms, flies and mice with improved GCaMP calcium indicators. *Nat Methods* **6**:875–881. doi:10.1038/nmeth.1398

Tobin DM, Madsen DM, Kahn-Kirby A, Peckol EL, Moulder G, Barstead R, Maricq A V., Bargmann CI. 2002. Combinatorial expression of TRPV channel proteins defines their sensory functions and subcellular localization in C. elegans neurons. *Neuron* **35**:307–

318. doi:10.1016/S0896-6273(02)00757-2

Ulanovsky N, Las L, Nelken I. 2003. Processing of low-probability sounds by cortical neurons. *Nat Neurosci* **6**:391–398. doi:10.1038/nn1032

White J., Southgate E, Thomson JN, Brenner S. 1986. The structure of the nervous sysytem o the nematode Caenorhabditis elegans. *Philos Trans ofthe R Soc B Biol Sci* **314**:1–340. doi:10.1126/science.7911601

Woolf CJ, Ma Q. 2007. Nociceptors-Noxious Stimulus Detectors. *Neuron* **55**:353–364. doi:10.1016/j.neuron.2007.07.016

Yamazaki SJ, Ohara K, Ito K, Kokubun N, Kitanishi T, Takaichi D, Yamada Y, Ikejiri Y, Hiramatsu F, Fujita K, Tanimoto Y, Yamazoe-Umemoto A, Hashimoto K, Sato K, Yoda K, Takahashi A, Ishikawa Y, Kamikouchi A, Hiryu S, Maekawa T, Kimura KD. 2019. SteftR: A hybrid versatile method for state estimation and feature extraction from the trajectory of animal behavior. *Front Neurosci* **13**. doi:10.3389/fnins.2019.00626

Yamazoe-Umemoto A, Fujita K, Iino Y, Iwasaki Y, Kimura KD. 2015. Modulation of different behavioral components by neuropeptide and dopamine signalings in non-associative odor learning of Caenorhabditis elegans. *Neurosci Res* **99**:22–33. doi:10.1016/j.neures.2015.05.009

Yeh E, Ng S, Zhang M, Bouhours M, Wang Y, Wang M, Hung W, Aoyagi K, Melnik-Martinez K, Li M, Liu F, Schafer WR, Zhen M. 2008. A putative cation channel, NCA-1, and a novel protein, UNC-80, transmit neuronal activity in C. elegans. *PLoS Biol* **6**:0552–0567. doi:10.1371/journal.pbio.0060055

Yemini E, Jucikas T, Grundy LJ, Brown AEX, Schafer WR. 2013. A database of Caenorhabditis elegans behavioral phenotypes. *Nat Methods* **10**:877–879. doi:10.1038/nmeth.2560

FIGURES AND TABLES

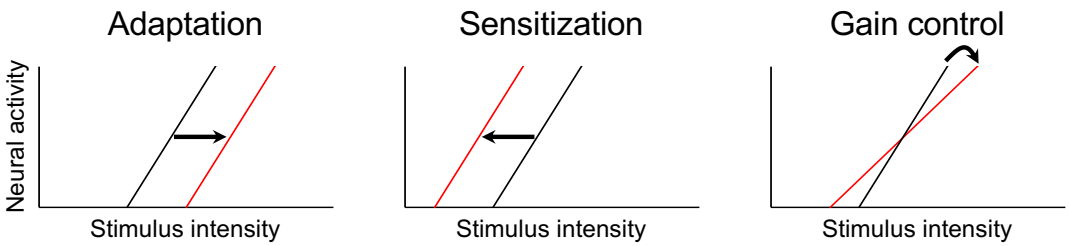


Figure 1: Schematic drawing of sensory modulations. Adaptation shifts the stimulus–response relationship to the right and sensitization shifts it to the left. Gain control is a change of its slope.

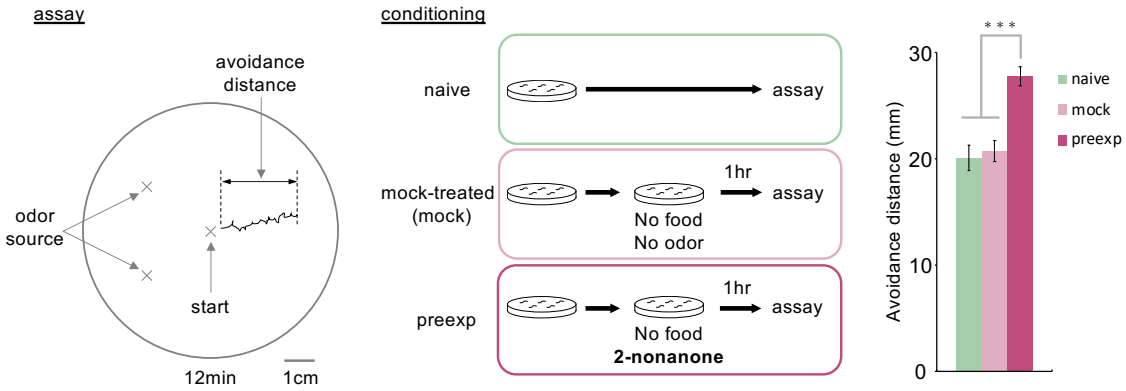


Figure 2: Preexposure to the repulsive odor 2-nonanone causes the enhancement of 2-nonanone avoidance. (left) Example of an animal's trajectory tracked during 12 minutes of 2-nonanone avoidance assay. (middle) The three conditions for 2-nonanone avoidance assay. (right) Result of 2-nonanone avoidance assay, where the average avoidance distance ± standard error in each condition is shown (n = 47, 45, 44 in naive, mock-treated, and preexposed conditions, respectively). Compared to control (*i.e.,* naive and mock-treated) animals, preexposed animals exhibit significantly longer avoidance distances. *** $p < 0.001$ (Kruskal-Wallis test with *post hoc* Steel-Dwass test).

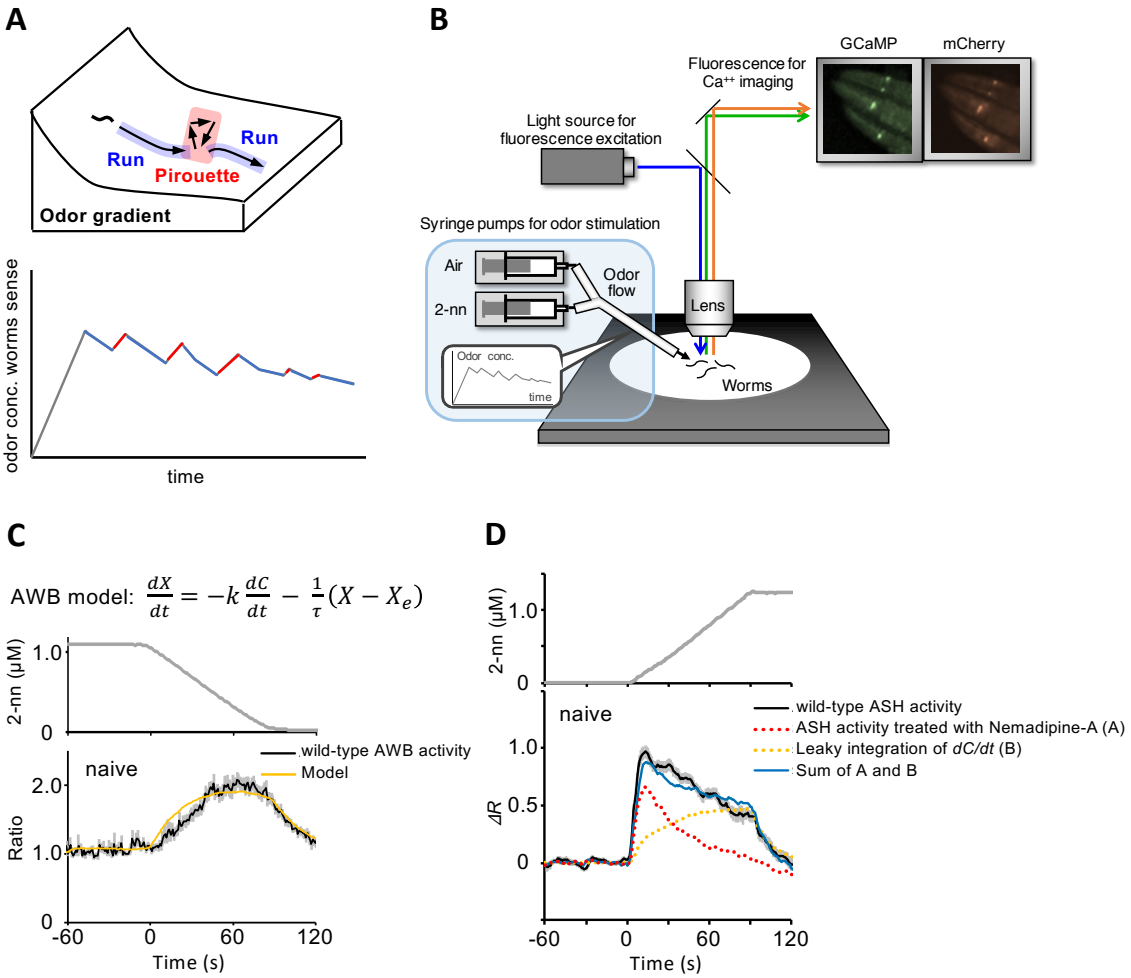


Figure 3: Behavioral and neuronal responses of *C. elegans* to the repulsive odor 2-nonanone. **A,** Odor concentration changes during avoidance behavior. (Top) Schematic drawing of a 2-nonanone gradient and the animals' behavioral states (runs and a pirouette) during the avoidance behavior. (Bottom) An example of odor concentration changes sensed by an animal during avoidance assay and the behavioral state during these changes. Runs (blue) and pirouettes (red) are mainly associated with a decrease and increase in odor concentration. In the initial phase of the assay (gray), the odor concentration always increases because the odor rapidly evaporates from its source. **B,** Schematic drawing of calcium imaging by the Kimura laboratory's original microscope system OSB2. Worms immobilized with the acetylcholine receptor antagonist levamisole were exposed to an odor flow, and the neural activities were monitored with dual color imaging. **C**, AWB response to a constant gradual decrease in 2-nonanone concentration. When a constant odor decrease (upper panel) is presented, AWB neurons in naive wild-type animals exhibit a gradually increasing response (black solid line in lower panel), which can be approximated by the leaky integration equation (top and yellow line in lower panel). The details of leaky integration equation are described in Materials and

Methods. **D**, ASH response to a constant gradual increase in 2-nonanone concentration. When a simple gradual odor increase (upper panel; odor gradient #1) is presented, ASH neurons in naive wild-type animals exhibit a fast and relatively constant response (black solid line in lower panel). In contrast, when wild-type animals are treated with Nemadipine-A, a specific antagonist for L-type VGCC EGL-19, ASH exhibits a fast and transient response (red dashed line in lower panel). Interestingly, when the transient response and the calculated leaky integration of time-differential of odor concentration mediated by the EGL-19 (yellow dashed line) are added (blue dashed line), the added result nicely reproduces the actual ASH response. For panel D, instead of the ratio (GCaMP/mCherry), ΔR (ratio - baseline) was used because in this panel, two different groups of wild-type ASH responses (untreated versus NemA-treated) were compared. Panels A–D are reproduced from the previous studies with some modifications (Tanimoto et al., 2017; Yamazaki et al., 2019).

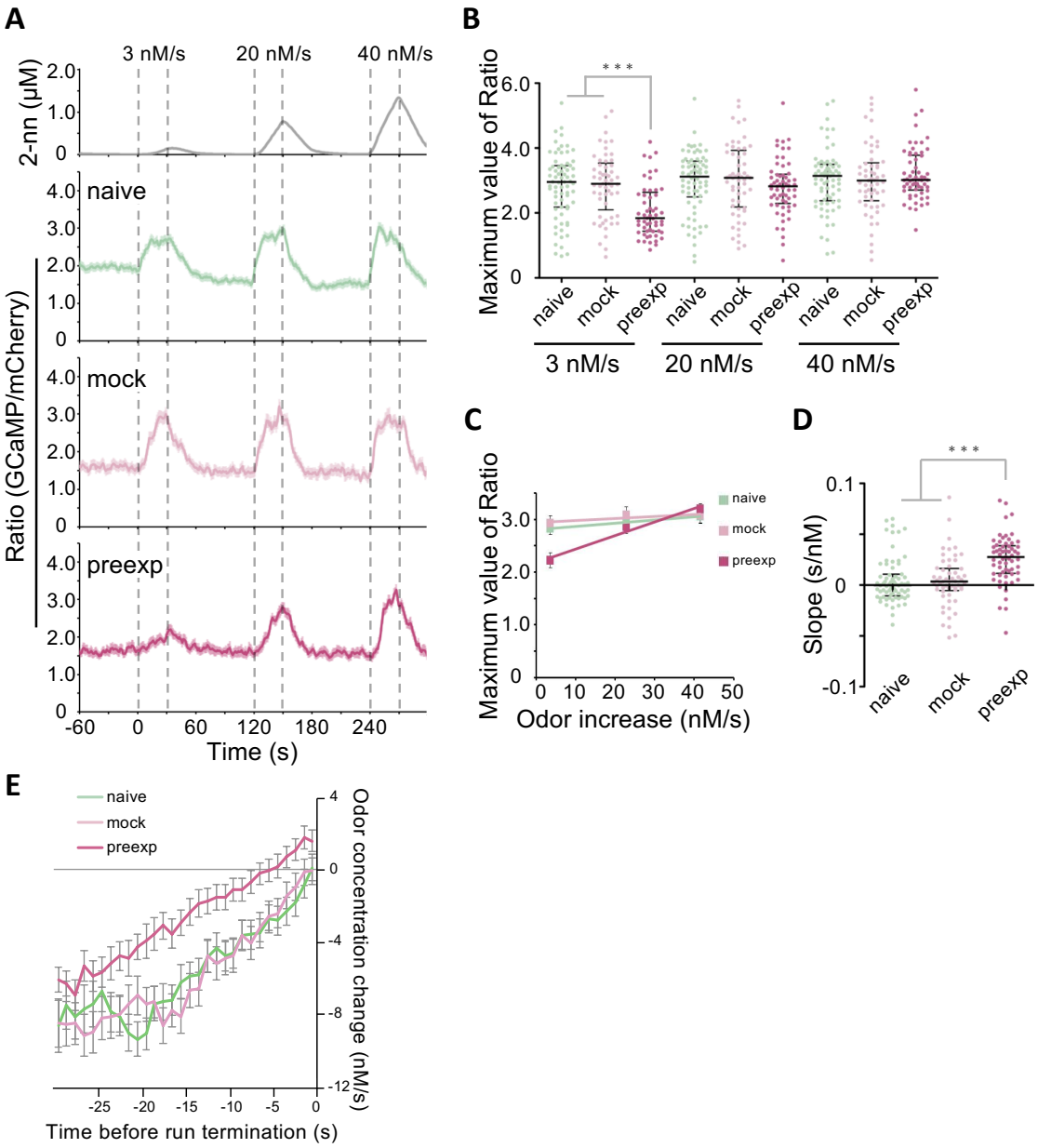


Figure 4: Preexposure to the repulsive odor 2-nonanone causes sensory gain control in ASH neurons. **A,** ASH responses to three consecutive stimuli (3, 20, and 40 nM/s; top) in the three conditions. In the naive (green) and mock-treated (pale red) conditions, the responses were always large regardless of the stimulus intensity. However, in the preexposure condition (dark red), the responses were smaller for small stimuli and larger for large stimuli. The solid lines and associated shadows are the average values and their standard errors, respectively (n = 71, 57, 61 in naive, mock-treated, and preexposed conditions, respectively). The black dotted lines indicate the onset and end of the odor increase phase. **B,** Scatter plot of the maximum values of ASH response (shown in panel A) to each stimulus. *** $p < 0.001$ (Kruskal-Wallis

test with *post hoc* Steel-Dwass test). **C**, Correlation between the rate of odor concentration increase and the maximum value of ASH response. The mean ± standard error of ASH maximum values in panel B and its linear approximation are shown. **D,** Scatter plot of the slope of the response. Each slope was calculated by linear approximation of maximum values of ASH responses of an animal to the three stimuli (3, 20, and 40 nM/s). *** $p < 0.001$ (Kruskal-Wallis test with *post hoc* Steel-Dwass test). **E**, Time-course changes of odor concentration that the animals sensed before the initiation of a pirouette. The odor concentrations that each animal sensed 30 seconds before the initiation were ensemble-averaged. The average values ± standard error of naive, mock-treated, and preexposed animals are shown in green, pale red and dark red, respectively (n = 50 in all conditions). In the naive and mock-treated animals, the transition from run to pirouette on average occurred when the average value of odor concentration change became close to zero, whereas the transition occurred several seconds after the animals started sensing increases in the odor concentration in the preexposed condition.

The behavioral analysis for panel E was performed by Shuhei Yamazaki.

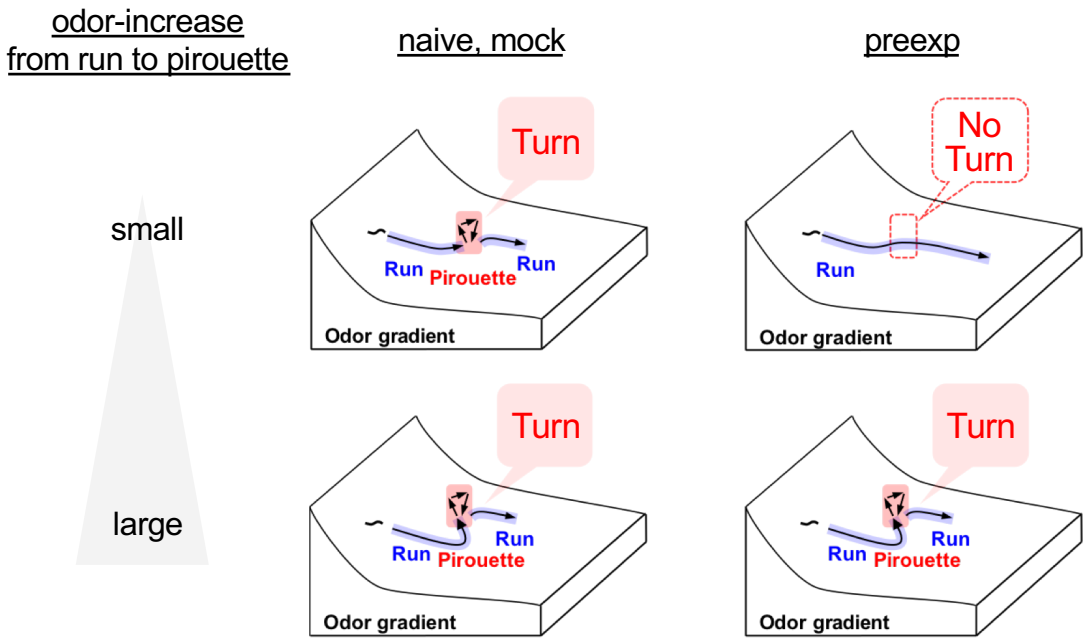


Figure 5: Cartoons of experience-dependent modulation of the odor avoidance behavior. An efficient repulsive behavior can be accomplished by suppressing only the response to a slight odor increase. A part of this figure has been published previously (Yamazaki et al., 2019).

A

$$X = k\frac{dC}{dt} + X_e$$

B

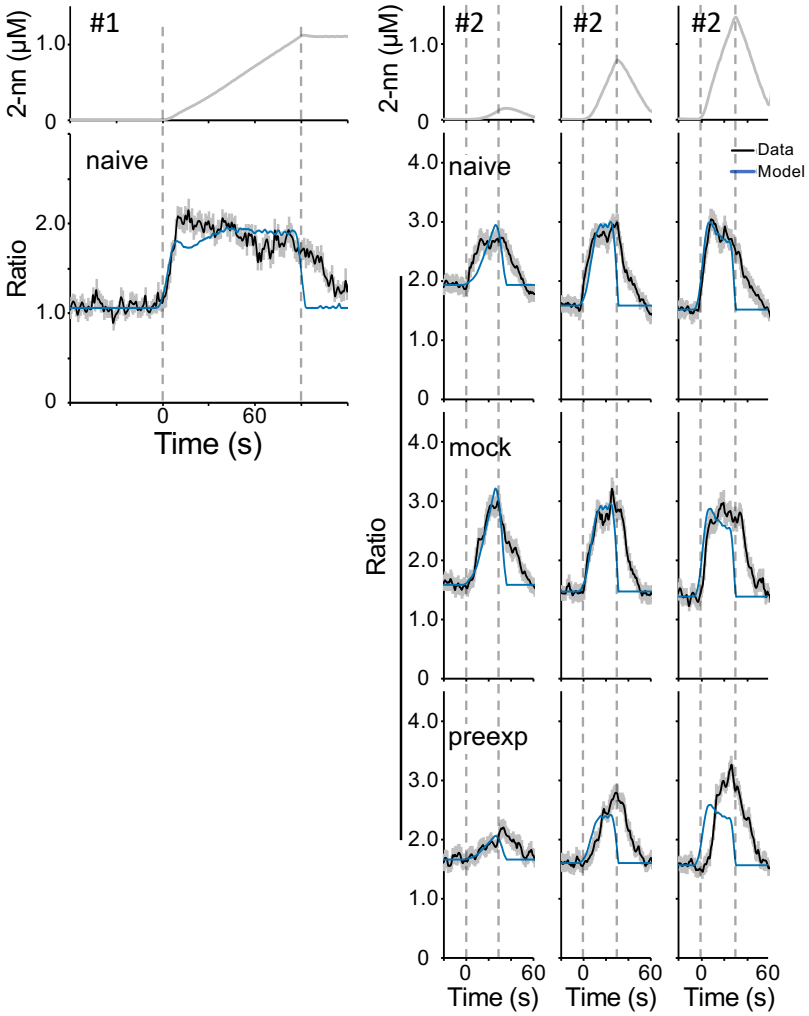


Figure 6: Independent fitting of the wild-type ASH response to the odor stimuli with the original simple time-differential model. **A,** Equation of the model. **B,** The fitting results of the ASH response to the odor gradient #1 (left) and to each stimulus of the odor gradient #2 (right). The black line indicates the actual ASH response and the blue line is the model. The black dotted line indicates the onset and end of the odor increase phase.

A

$$\frac{dX}{dt} = k_1 \frac{dC}{dt} - \frac{1}{\tau}(X - X_e)$$

B

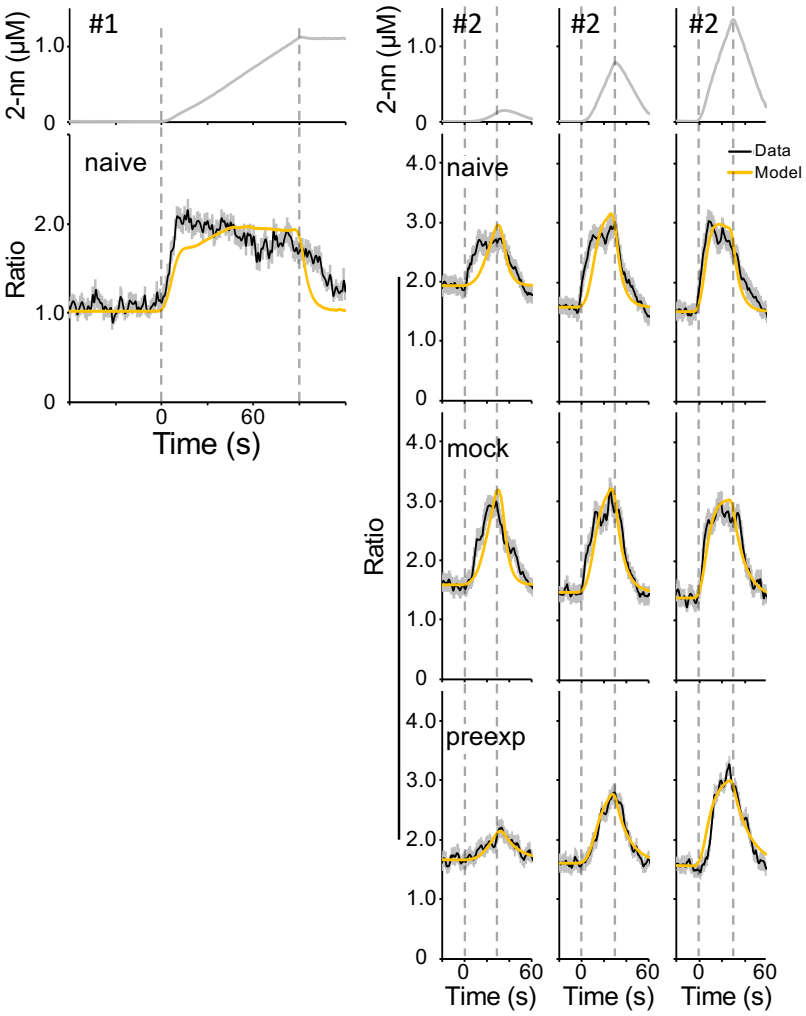


Figure 7: Independent fitting of the wild-type ASH response to the odor stimuli with the leaky integration of first-order time-differential model. **A,** Equation of the model. **B,** The fitting results of the ASH response to the odor gradient #1 (left) and to each stimulus of the odor gradient #2 (right). The black line indicates the actual ASH response and the yellow line is the model. The black dotted line indicates the onset and end of the odor increase phase.

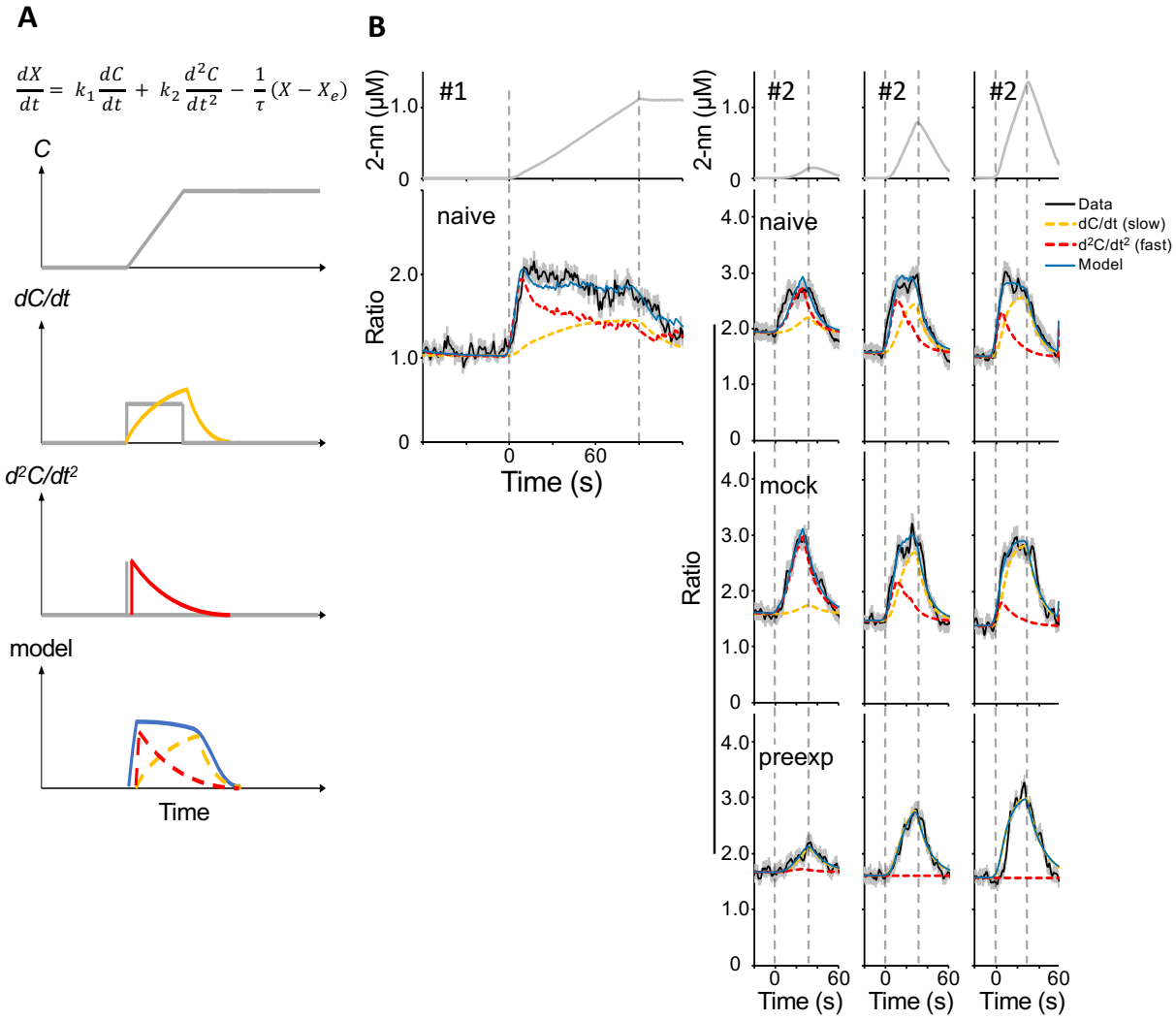


Figure 8: Mathematical model of wild-type ASH response independently fitted to a single odor stimulus. **A,** Schematic drawing of a mathematical model of ASH response. Equation of the first and second differential model is shown at the top. Also shown are the time course of a simple gradual odor concentration increase (top panel), first-order time-differential of odor concentration and its leaky integration (gray rectangle and yellow line, respectively, in the second panel), second-order time-differential of the odor concentration and its leaky integration (gray vertical bar and red line, respectively, in the third panel; negative value of second-order time-differential is not calculated), and the sum of leaky integration of first- and second-order time-differentials (blue solid, yellow dashed and red dashed lines, respectively, in the bottom panel). **B,** The results of fitting the ASH response to the simple gradual odor increase used in the previous study (left; odor gradient #1, n = 39) and independent fitting to each of three consecutive odor stimuli used in Figure 4A (right; odor gradient #2, n = 71, 57,

61 in naive, mock-treated, and preexposed conditions, respectively). The top panels exhibit each odor concentration change, and lower panels exhibit ASH responses of different conditions of animals (naive, mock-treated or preexposed) to each stimulus. The black line and the associated gray area are the average ASH responses and their standard errors, the blue line is the model, the yellow and red dashed lines are the first- and second-order components in the model, respectively. The black dotted line indicates the onset and end of the odor increase phase.

A

$$\frac{dX}{dt} = k_2 \frac{d^2C}{dt^2} - \frac{1}{\tau}(X - X_e)$$

B

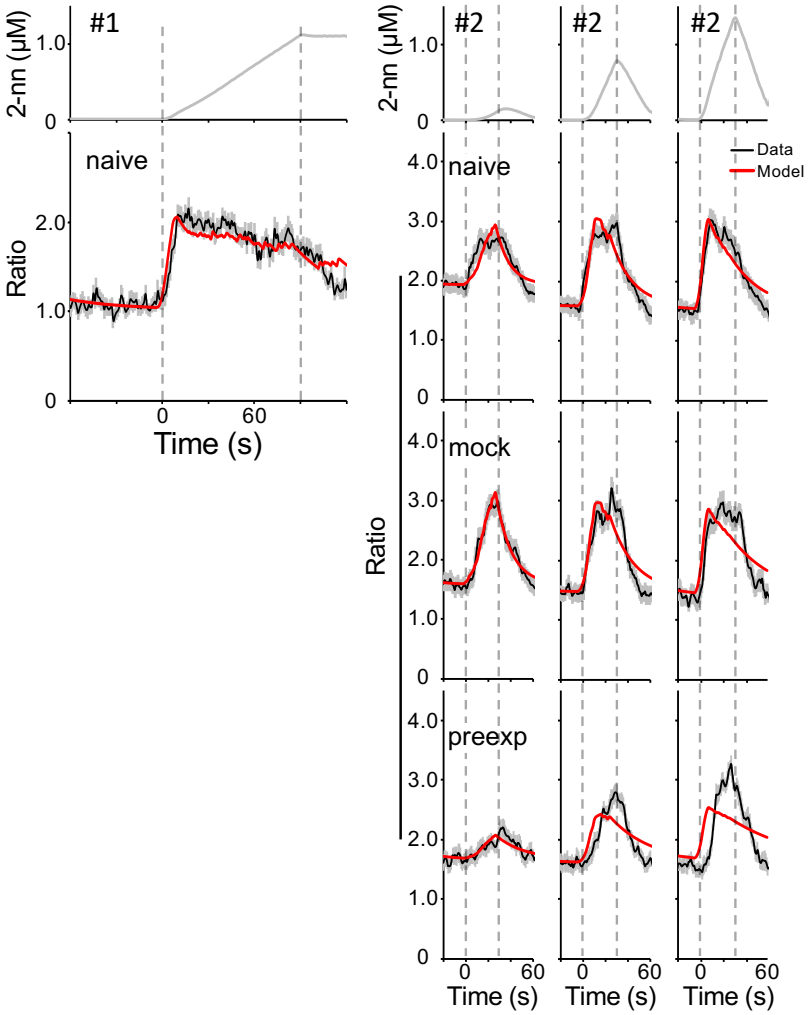


Figure 9: Independent fitting of the wild-type ASH response to the odor stimuli with the leaky integration of second-order time-differential model. **A,** Equation of the model. **B,** The fitting results of the ASH response to the odor gradient #1 (left) and to each stimulus of the odor gradient #2 (right). The black line indicates the actual ASH response and the red line is the model. The black dotted line indicates the onset and end of the odor increase phase.

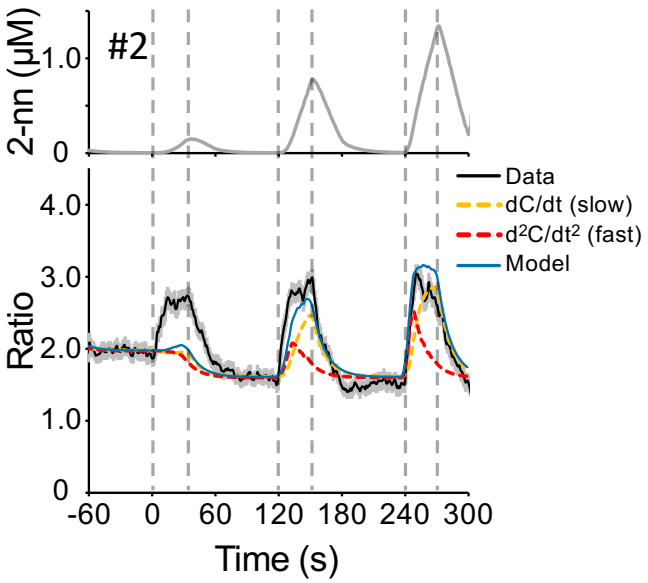


Figure 10: Fitting of the model with constant parameters for whole naive ASH response to the odor gradient #2. The model was fitted through all odor stimuli based on the least-squares method. The responses to 20 nM/s and 40 nM/s increases were well reproduced while the one to 3 nM/s increase was not.

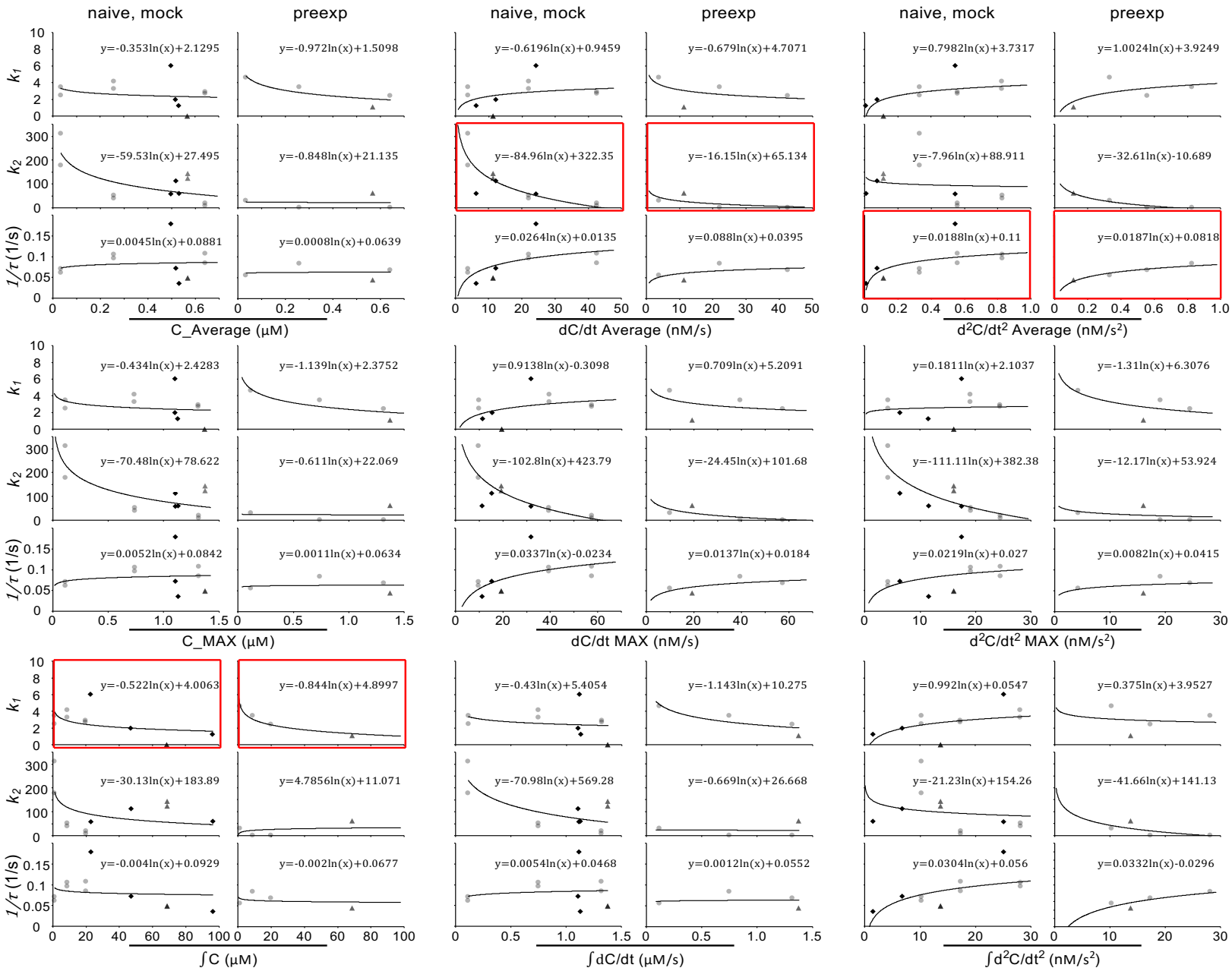

naive, mock
preexp
naive, mock
preexp
naive, mock
preexp
k1
k2
1/τ (1/s)
y=-0.353ln(x)+2.1295
y=-0.972ln(x)+1.5098
y=-0.6196ln(x)+0.9459
y=-0.679ln(x)+4.7071
y=0.7982ln(x)+3.7317
y=1.0024ln(x)+3.9249
y=-59.53ln(x)+27.495
y=-0.848ln(x)+21.135
y=-84.96ln(x)+322.35
y=-16.15ln(x)+65.134
y=-7.96ln(x)+88.911
y=-32.61ln(x)-10.689
y=0.0045ln(x)+0.0881
y=0.0008ln(x)+0.0639
y=0.0264ln(x)+0.0135
y=0.088ln(x)+0.0395
y=0.0188ln(x)+0.11
y=0.0187ln(x)+0.0818
C_Average (μM)
dC/dt Average (nM/s)
d²C/dt² Average (nM/s²)
y=-0.434ln(x)+2.4283
y=-1.139ln(x)+2.3752
y=0.9138ln(x)-0.3098
y=0.709ln(x)+5.2091
y=0.1811ln(x)+2.1037
y=-1.31ln(x)+6.3076
y=-70.48ln(x)+78.622
y=-0.611ln(x)+22.069
y=-102.8ln(x)+423.79
y=-24.45ln(x)+101.68
y=-111.11ln(x)+382.38
y=-12.17ln(x)+53.924
y=0.0052ln(x)+0.0842
y=0.0011ln(x)+0.0634
y=0.0337ln(x)-0.0234
y=0.0137ln(x)+0.0184
y=0.0219ln(x)+0.027
y=0.0082ln(x)+0.0415
C_MAX (μM)
dC/dt MAX (nM/s)
d²C/dt² MAX (nM/s²)
y=-0.522ln(x)+4.0063
y=-0.844ln(x)+4.8997
y=-0.43ln(x)+5.4054
y=-1.143ln(x)+10.275
y=0.992ln(x)+0.0547
y=0.375ln(x)+3.9527
y=-30.13ln(x)+183.89
y=4.7856ln(x)+11.071
y=-70.98ln(x)+569.28
y=-0.669ln(x)+26.668
y=-21.23ln(x)+154.26
y=-41.66ln(x)+141.13
y=-0.004ln(x)+0.0929
y=-0.002ln(x)+0.0677
y=0.0054ln(x)+0.0468
y=0.0012ln(x)+0.0552
y=0.0304ln(x)+0.056
y=0.0332ln(x)-0.0296
∫C (μM)
∫dC/dt (μM/s)
∫d²C/dt² (nM/s²)

Figure 11: Scatter plots of the relationship between each aspect of stimuli and parameter. I plotted the relationship between the parameters that reproduced the ASH response to each odor increase and their inputs (average, maximum and integrated value of odor concentration, first-order time-differential of odor concentration, and second-order time-differential of odor concentration). Black rhombuses, light gray circles, and dark gray triangles represent ASH responses to odor gradient #1, #2, and #3, respectively. The relationships finally chosen (Figure 12A) are indicated by red rectangles.

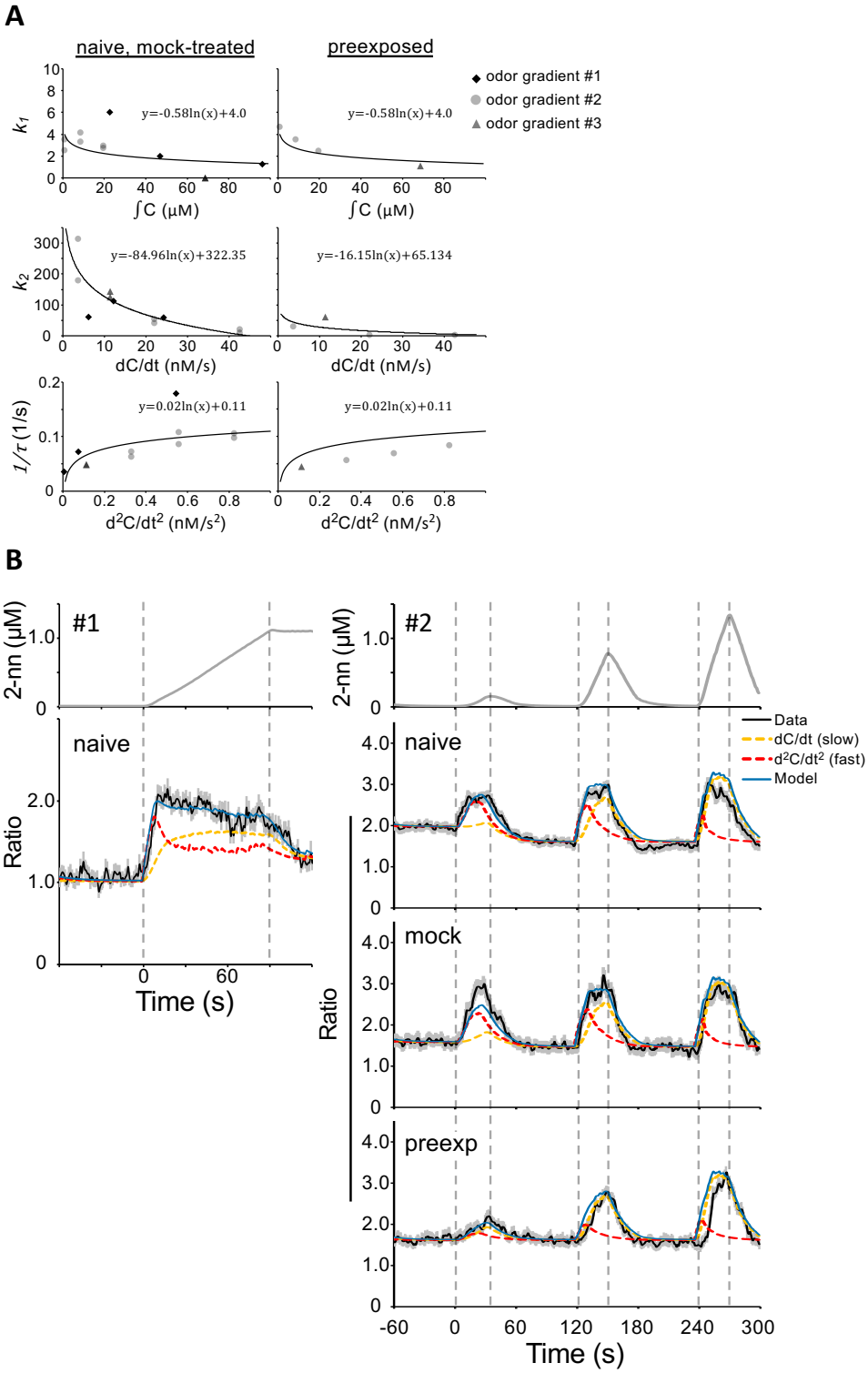


Figure 12: Model of wild-type ASH response fitted to the odor gradient #1 and #2 with stimulus-dependent parameters. **A,** Scatter plots used for the first and second differential model with stimulus-dependent parameters. Only the parameter of the second-order time-differential, k_2, is substantially different between naive, and mock-treated versus preexposed conditions. Black rhombuses, light gray circles, and dark gray triangles represent each ASH response to odor gradient #1, #2, and #3, respectively. Odor gradient #3 was used for the

genetic analysis (Figure 13). **B,** ASH response and its model to a simple odor increase (left ; odor gradient #1, n = 39) and to the three consecutive stimuli (right; odor gradient #2, n = 71, 57, 61 in naive, mock-treated, and preexposed conditions, respectively). The black line and the associated gray area are the average ASH responses and their standard errors, the blue line is the model, the yellow and red dashed lines are the first- and second-order component in the model, respectively. The black dotted line indicates the onset and end of the odor increase phase.

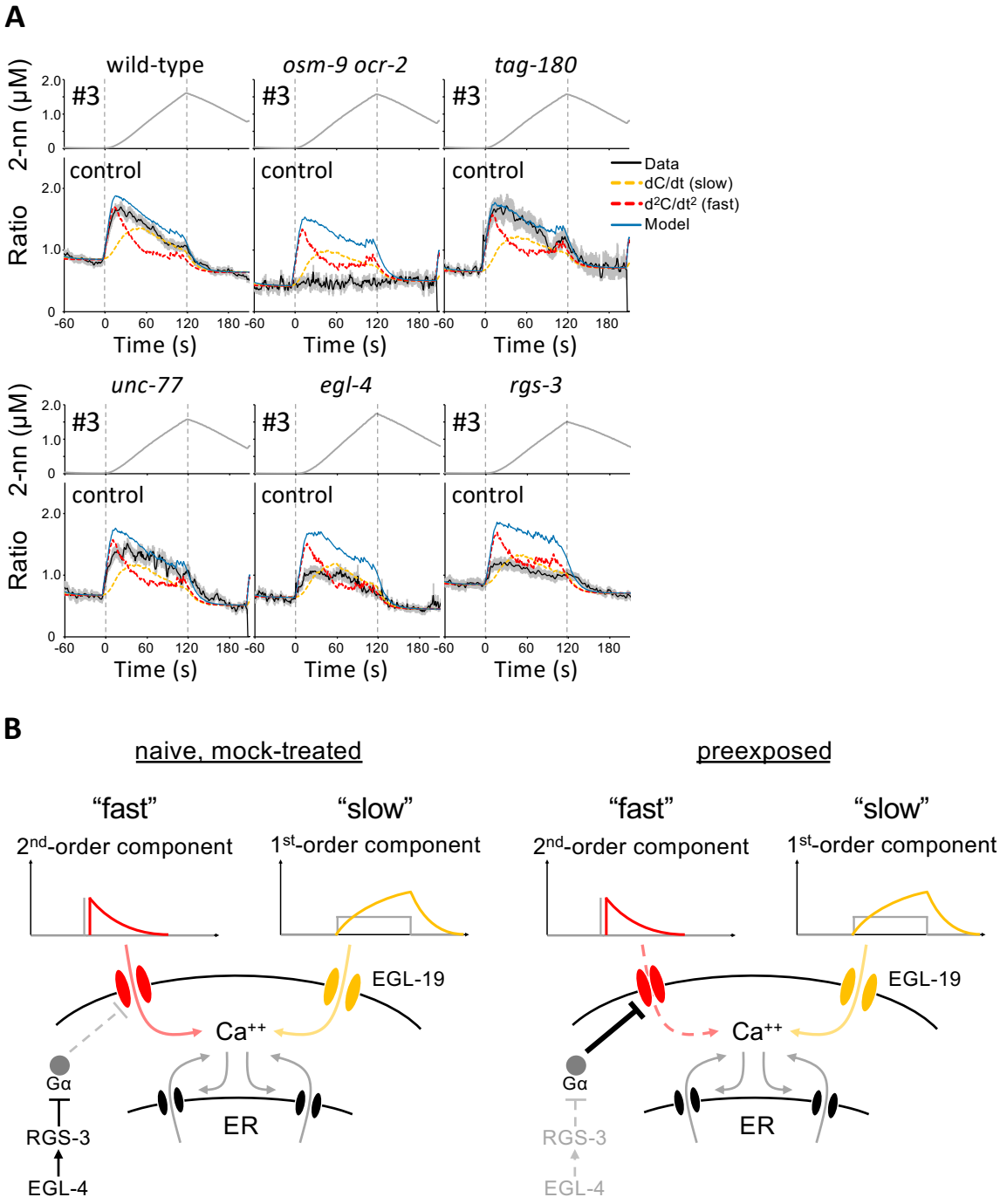


Figure 13: Genetic analysis of the ASH gain control. **A**, ASH response in wild-type and mutant animals in control condition (n =51 in wild-type; n = 7 in *osm-9 ocr-2*; n = 15 in *tag-180*; n = 16 in *unc-77*; n = 46 in *egl-4*; n = 29 in *rgs-3*) to a longer and larger continuous odor increase (up to ~2 µM within 120 s; odor gradient #3). This odor stimulus was used because of the idea that even milder mutant phenotypes would be observed clearly with a longer and larger stimulus. The black line and the associated gray area are the average ASH responses and their standard errors. The model parameters to fit for the wild-type response in Figure 12

were used, and overlayed with each of the ASH responses. The black dotted line indicates the onset and end of the odor increase phase. **B**, A proposed molecular model of ASH response. ASH response is mainly mediated by transiently active calcium channels (red) and persistently active L-type VGCCs (yellow). Gα protein activity can suppress the transiently active calcium channels, and this Gα protein activity is inhibited by PKG–RGS pathway in naive/mock-treated conditions. Gain control is caused only by suppression of the transiently active calcium channels via the Gα signaling. The calcium influx from the plasma membrane is further increased by the calcium-induced calcium release through IP3 receptor and ryanodine receptor on ER membrane (Tanimoto et al., 2017).
The calcium imaging experiment for mutants was performed by Yuto Endo.

Table 1. Comparison of BIC for linear and logarithmic approximation of stimulus-dependent parameters

Odor	#1	#2		
Condition	Naive	Naive	Mock-treated	Preexp
Linear approximation	-539.2	-899.6	-1009	-682.0
Logarithmic approximation	**-778.4**	**-1135**	**-1116**	**-966.9**

The conditions with the smallest BIC values under each condition are indicated in bold. In all the conditions, the model with a logarithmic approximation has a better BIC value than the model with a linear approximation.

Table 2. Summary of comparing BIC value among mathematical models

Odor	#1	3nM/s increase in #2			20nM/s increase in #2			40nM/s increase in #2		
Condition	Naive	Naive	Mock-treated	Preexp	Naive	Mock-treated	Preexp	Naive	Mock-treated	Preexp
$X = k\frac{dC}{dt} + X_e$	-557.3	-216.9	-195.0	-278.5	-153.5	-125.8	-140.8	-158.9	-92.5	-68.8
$\frac{dX}{dt} = k_1\frac{dC}{dt} - \tau(X - X_e)$	-559.9	-240.4	-217.7	**-423.4**	-205.0	-233.8	**-379.2**	-235.6	-260.8	**-261.5**
$\frac{dX}{dt} = k_2\frac{d^2C}{dt^2} - \tau(X - X_e)$	-741.1	**-287.6**	**-368.6**	-373.8	-253.5	-211.6	-211.3	-224.4	-159.4	-109.7
$\frac{dX}{dt} = k_1\frac{dC}{dt} + k_2\frac{d^2C}{dt^2} - \tau(X - X_e)$	**-769.6**	-286.5	-366.7	-420.5	**-301.2**	**-298.1**	-374.8	**-336.3**	**-289.0**	-257.1

BIC values were calculated independently for each odor stimulus. The conditions with the smallest BIC values under each condition are indicated in bold.

Table 3. Summary of BIC value for the ASH mathematical model in mutants.

Genotype	N2	*osm-9ocr-2*	*tag-180*	*unc-77*	*egl-4*	*rgs-3*
$\frac{dX}{dt} = k_1 \frac{dC}{dt} - \tau(X - X_e)$	-800.0	**-654.8**	-652.5	-818.6	**-1171**	**-1055**
$\frac{dX}{dt} = k_2 \frac{d^2C}{dt^2} - \tau(X - X_e)$	-768.0	-587.7	-737.4	-795.5	-987.8	-896.7
$\frac{dX}{dt} = k_1 \frac{dC}{dt} + k_2 \frac{d^2C}{dt^2} - \tau(X - X_e)$	**-899.7**	-260.2	**-1171**	**-960.8**	-530.4	-454.2

The conditions with the smallest BIC values under each condition are indicated in bold.

ACKNOWLEDGEMENTS

I would like to express my deepest gratitude to Prof. Kotaro Kimura for supervising all the aspects of my study. I also deeply thank for Drs. Koichi Fujimoto, Yasushi Iwatani, Yuki Tsukada and Yuishi Iwasaki for generous cooperation about mathematical modeling. I am greatful to Drs. Sakiko Shiga, Masahiro Ueda, and the Kimura laboratory members for their valuable advice, comments and technical assistance for this study. Nematode strains were provided by the Caenorhabditis Genetics Center. Lastly, I also greatly thank my family and friends for their understanding and support.

PUBLICATIONS AND PRESENTATIONS

Publication

1) Ikejiri Y, Tanimoto Y, Fujita K, Hiramatsu F, Yamazaki SJ, Endo Y, Iwatani Y, Fujimoto K, Kimura KD. Neural mechanism of experience-dependent sensory gain control in *C. elegans*. eLife. submitted

Presentations

1) Learning-dependent changes in nociceptive neuron activity in the nematode *C. elegans*, The 40th Annual Meeting of the Japan Neuroscience Society, Chiba, 2017

2) Learning-dependent neural gain control by asymmetric modulation of first- and second-order time-differential of stimulus in sensory neurons, Ceneuro2018, Madison, 2018

3) Mechanism of learning-dependent activity changes in sensory neurons in *Caenorhabditis elegans*, The 41st Annual Meeting of the Japan Neuroscience Society, Kobe, 2018

4) Learning-dependent gain control by asymmetric modulation of the first- and second-order time-differential of stimulus in sensory neurons, 23rd International *C. elegans* Conference, Online, 2021